Inhibition of SARS-CoV-2 infection in human iPSC-derived cardiomyocytes by targeting the Sigma-1 receptor disrupts cytoarchitecture and beating

José Alexandre Salerno[1,2†], Thayana Torquato[1†], Jairo R. Temerozo[3,4], Livia Goto-Silva[1], Karina Karmirian[1,2], Mayara A. Mendes[1], Carolina Q. Sacramento[5,6], Natalia Fintelman-Rodrigues[5,6], Letícia R Q Souza[1], Isis M Ornelas[1], Carla P Veríssimo[2], Luiz Guilherme H S Aragão[1], Gabriela Vitória[1], Carolina SG Pedrosa[1], Suelen da Silva Gomes Dias[5], Vinicius Cardoso Soares[2,5], Teresa Puig-Pijuan[1,7], Vinícius Salazar[8], Rafael Dariolli[9,10], Diogo Biagi[10], Daniel Rodrigues Furtado[1], Luciana Barreto Chiarini[7], Helena L. Borges[2], Patrícia T. Bozza[5], Marília Zaluar P. Guimarães[1,2], Thiago M L Souza[5,6], Stevens K. Rehen[1,11*].

[1] D'Or Institute for Research and Education (IDOR), Rio de Janeiro, Brazil.
[2] Institute of Biomedical Sciences, Federal University of Rio de Janeiro (UFRJ), Rio de Janeiro, Brazil.
[3] National Institute for Science and Technology on Neuroimmunomodulation (INCT/NIM), Oswaldo Cruz Institute (IOC), Oswaldo Cruz Foundation (Fiocruz), Rio de Janeiro, Brazil.
[4] Laboratory on Thymus Research, Oswaldo Cruz Institute (IOC), Oswaldo Cruz Foundation (Fiocruz), Rio de Janeiro, Brazil.
[5] Immunopharmacology Laboratory, Oswaldo Cruz Institute (IOC), Oswaldo Cruz Foundation (Fiocruz), Rio de Janeiro, Brazil.
[6] National Institute for Science and Technology on Innovation in Diseases of Neglected Populations (INCT/IDPN), Center for Technological Development in Health (CDTS), Oswaldo Cruz Foundation (Fiocruz), Rio de Janeiro, Brazil.
[7] Carlos Chagas Filho Institute of Biophysics (IBCCF), Federal University of Rio de Janeiro (UFRJ), Rio de Janeiro, Brazil.
[8] Department of Systems and Computer Engineering, COPPE, Federal University of Rio de Janeiro (UFRJ), Rio de Janeiro, Brazil.
[9] Department of Pharmacological Sciences, Icahn School of Medicine at Mount Sinai, New York, NY, USA
[10] Pluricell Biotech, São Paulo, Brazil.
[11] Department of Genetics, Institute of Biology, Federal University of Rio de Janeiro (UFRJ), Rio de Janeiro, Brazil.

Corresponding Author:
Stevens K. Rehen[1,11]
Diniz Cordeiro 30, Rio de Janeiro, Rio de Janeiro/RJ, 22281-100, Brazil
Email address: srehen@lance-ufrj.org

Abstract

SARS-CoV-2 infects cardiac cells and causes heart dysfunction. Conditions such as myocarditis and arrhythmia have been reported in COVID-19 patients. The Sigma-1 receptor (S1R) is a ubiquitously expressed chaperone that plays a central role in cardiomyocyte function. S1R has been proposed as a therapeutic target because it may affect SARS-CoV-2 replication, however, the impact of the inhibition of S1R in human cardiomyocytes remains to be described. In this study, we investigated the consequences of S1R inhibition in iPS-derived human cardiomyocytes (hiPSC-CM). SARS-CoV-2 infection in hiPSC-CM was productive and reduced cell survival. S1R inhibition decreased both the number of infected cells and viral particles after 48 hours. S1R inhibition also prevented the release of pro-inflammatory cytokines and cell death. Although the S1R antagonist NE-100 triggered those protective effects, it compromised cytoskeleton integrity by downregulating the expression of structural-related genes and reducing beating frequency. Our findings suggest that the detrimental effects of S1R inhibition in human cardiomyocytes' integrity may abrogate its therapeutic potential against COVID and should be carefully considered.

Introduction

COVID-19 is an airborne infectious disease caused by the Severe Acute Respiratory Syndrome Coronavirus 2 (SARS-CoV-2). Since the first patients were diagnosed, myocardial injury following SARS-CoV-2 infection has been reported increasing the in-hospital mortality (of 51.2%) in comparison to cases without cardiac injury (of 4.5%) (Huang et al., 2020; Gnecchi et al., 2020; Shi et al., 2020). Pre-existing cardiovascular comorbidities are related to worse clinical outcomes and, together with diabetes, are the most common chronic conditions among hospitalized COVID-19 patients (Yang et al., 2020; Magadum & Kishore, 2020). Hence, there is a higher prevalence of cardiovascular complications as extrapulmonary COVID-19. Together, these data reinforce that therapeutic approaches targeting SARS-CoV-2 infection must not only seek to diminish cardiac damage by COVID-19, but also consider the eventual drug-induced damage to the heart, which would in turn aggravate the disease (Pellicori et al., 2021).

Human induced pluripotent stem cell-derived cardiomyocytes (hiPSC-CMs) reproduce key features of human myocardial cells, such as expression of lineage-specific markers, sarcomeric and cytoskeletal organization, subcellular structures, and contractility (Karakikes et al., 2015). Given the scarcity of cardiomyocytes from other sources and the suitability of hiPSC-CMs as a model *in vitro* for cardiac diseases, they are useful tools to investigate SARS-CoV-2 infection and to test drugs that may eventually prevent cardiac susceptibility. Indeed they were used for these purposes and it was shown that the new coronavirus infects these cells and causes mechanical and electrical impairment (Sharma et al., 2020; Choi et al., 2020; Wong et al., 2020; Perez-Bermejo et al., 2021; Marchiano et al., 2021). Also, these cells are reliable to evaluate drug-induced cardiotoxicity, which is one of the main causes of drug withdrawal from the market due to fatal side effects (Chaudhari et al., 2016; Sharma et al., 2018; Choi et al., 2020). hiPSC-

79 CMs can be used as a preclinical model to investigate the safety of emerging therapeutics and
80 more effective treatments for COVID-19.

81

82 Compounds from drug repurposing studies have been proposed to display antiviral activity
83 against SARS-CoV-2 (Lovato et al., 2020). Negative modulators of the Sigma-1 receptor (S1R)
84 interact with the Non-Structural Protein 6 (NSP6) from SARS-CoV-2 (Gordon et al., 2020b;
85 Hashimoto, 2021). Knockout of S1R decreased the replication of SARS-CoV-2 in Caco-2 cells
86 (Gordon et al., 2020a). The NSP6 is one of the proteins assembled into the replication complex
87 built in the endoplasmic reticulum (ER) of host cells infected by other coronaviruses (Cottam et
88 al., 2011a; Cottam, Whelband & Wileman, 2014). The role of NSP6 in the intracellular viral
89 cycle has been associated with the formation of vesicles in sites of replication and
90 autophagosomes to favor the replication in the ER and ER-derived vesicles (Cottam et al.,
91 2011b; Cottam, Whelband & Wileman, 2014). Interestingly, this is the subcellular localization
92 where S1R is enriched, especially within the ER-mitochondrion contact (Dussossoy et al., 1999;
93 Hayashi & Su, 2003a,b, 2007; Su et al., 2010; Brune, Pricl & Wünsch, 2013; Rousseaux &
94 Greene, 2016; Gordon et al., 2020b). However, this receptor is an ER chaperone that acts
95 assisting in the folding of host proteins, either during their synthesis or function, and controlling
96 calcium homeostasis (Morales-Lázaro, González-Ramírez & Rosenbaum, 2019). S1R is also a
97 key intracellular amplifier of signal transduction in different pathways including bioenergetics
98 and response to cellular stress (Hayashi & Su, 2007; Hayashi et al., 2009; Hayashi, 2015).
99 Therefore, although targeting this receptor was shown to block SARS-CoV-2 replication, it may
100 also lead to harmful side effects because of its involvement in vital cellular functions.

101

102 In the context of cardiac tissue, S1R plays important roles in cardioprotection against
103 maladaptive ER stress responses, apoptosis after ischemic injuries and hypertrophy (Tagashira &
104 Fukunaga, 2012; Tagashira et al., 2013, 2014; Hirano, Tagashira & Fukunaga, 2014; Lewis et al.,
105 2020). Research both *in vivo* and *in vitro* have proposed calcium homeostasis and suppression of
106 ER stress induced toxicity as possible events related to S1R cardiovascular function in rodents
107 (Bhuiyan & Fukunaga, 2009; Tagashira et al., 2013; Shinoda et al., 2016a; Qin et al., 2019).
108 Accordingly, depletion of S1R has been demonstrated to cause mitochondrial damage and
109 contractile dysfunction (Abdullah et al., 2018, 2020).

110

111 Drugs that bind to Sigma receptors, even as an off-target, have been considered as potential
112 therapeutics to prevent or to treat COVID-19 (Reznikov et al., 2020; Vela, 2020). Some of these
113 compounds have been reported to exhibit antiviral activity against other coronaviruses, together
114 with cardiotoxicity and induction of arrhythmias (Chen, Wang & Lin, 2006; Page et al., 2016).
115 Others, however, have stated that the antiviral properties of these compounds are due to their
116 physicochemical properties rather than their pharmacological interaction with S1R (Tummino et
117 al., 2021). Therefore, the modulation of S1R is in the spotlight of alternative approaches to treat
118 COVID-19 but it remains to be explored in the perspective of efficiency and safety in human

119 heart cells. In this study, we investigated the consequences of the inhibition of S1R in hiPSC-
120 CMs. Inhibition of S1R led to transcriptional modifications of myofibril-associated genes,
121 aberrant changes in the cytoskeleton and decreased beating frequency, despite reducing infection
122 and viral replication of SARS-CoV-2 and preventing viral-associated cytokine release and cell
123 death. These results provide new insights about targeting S1R as a strategy against COVID-19
124 and possible adverse cardiac outcomes.

125

Materials & Methods

127 hiPSC-CMs culture
128 Fresh human iPSCs-derived cardiomyocytes were purchased from Pluricell (São Paulo, Brazil)
129 and the protocol for cardiomyocyte differentiation is described (Cruvinel et al., 2020). Upon
130 arrival, cardiomyocytes were allowed to regain contractility and maintained at 37°C in a
131 humidified atmosphere with 5% CO2. Cardiomyocytes were used between days 30 to 40 of
132 differentiation.

133

134 Chemicals
135 4-Methoxy-3-(2-phenylethoxy)-N,N-dipropylbenzeneethanamine hydrochloride (NE-100
136 hydrochloride) was purchased from Tocris (3133). Stock and work solutions were prepared using
137 100% dimethyl sulfoxide sterile-filtered (DMSO; D2650 - Sigma-Aldrich).

138

139 Flow Cytometry
140 Cardiomyocytes were plated on 6-well plates coated with GELTREX and cultivated for 7 days.
141 After cell dissociation, cells were fixed with 1% paraformaldehyde (PFA), permeabilized with
142 Triton 0.1% (Sigma Aldrich) and Saponin 0.1% (Sigma Aldrich) and stained with the antibodies
143 anti-TNNT2 (1:2500; Thermo Fisher, MA5-12960) and anti-OCT4 (1:200, Thermo Fisher,
144 MA5-14845). FC data was acquired using a Canto BD flow cytometer for each batch of
145 differentiation and analyzed using the FlowJo Software considering 1%–2% of false-positive
146 events.

147

148 SARS-CoV-2 Propagation
149 SARS-CoV-2 was expanded in Vero E6 cells from an isolate obtained from a nasopharyngeal
150 swab of a confirmed case in Rio de Janeiro, Brazil (GenBank accession no. MT710714). The
151 National Review Board approved the study protocol (CONEP 30650420.4.1001.0008) for
152 clinical samples, and informed consent was obtained from all participants or patients'
153 representatives. Viral isolation was performed after a single passage in cell culture in 150 cm^2
154 flasks with high glucose DMEM 2% FBS. Observations for cytopathic effects were performed
155 daily and peaked 4 to 5 days after infection. All procedures related to virus culture were handled
156 in biosafety level 3 (BSL3) multi-user facilities according to WHO guidelines. Virus titers were
157 determined as plaque-forming units (PFU), and virus stocks were kept in -80°C ultra-low
158 temperature freezers.

159 Infections and virus titration
160 Cardiomyocytes were infected with SARS-CoV-2 at MOI of 0.1 in CDM3 media without serum.
161 After 1 hour, cells were washed and incubated with complete medium with treatments or not. For
162 virus titration, monolayers of Vero E6 cells (2×10^4 cells/well) in 96-well plates were infected
163 with serial dilutions of supernatants containing SARS-CoV-2 for 1 hour at 37°C. A semi-solid
164 high glucose DMEM medium containing 2% FSB and 2.4% carboxymethylcellulose was added
165 and cultures were incubated for 3 days at 37°C. Then, cells were fixed with 10% formalin for 2 h
166 at room temperature. The cell monolayer was stained with 0.04% solution of crystal violet in
167 20% ethanol for 1 h. Plaque numbers were scored in at least 3 replicates per dilution by
168 independent readers blinded to the experimental group and the virus titers were determined by
169 PFU per milliliter (PFU/ml).
170
171 Immunocytochemistry and Fluorescence Image Analysis
172 Cells were fixed using 4% PFA solution (Sigma-Aldrich) for 1 h, washed with 1X PBS and then
173 incubated with permeabilization/blocking solution (0.3% Triton X-100/3% bovine serum
174 albumin) for 1 h. Primary antibodies were diluted in blocking solution and incubated at 4ºC
175 overnight, namely anti-SARS-CoV-2 convalescent serum (1:1000); anti-SARS-CoV-2 spike
176 protein monoclonal antibody (SP) (1:500, G632604 - Genetex); anti-cardiac troponin T (cTnT)
177 (1:500, MA5-12960 - Invitrogen), anti-VDAC1/Porin (1:100, ab34726 – Abcam), anti-Calnexin
178 (1:50, #2433 – Cell Signaling Technology) and anti-Sigma1R B-5 (1:100, SC-137075 - Santa
179 Cruz Biotechnology). The use of the convalescent serum from COVID-19 patients was approved
180 by CAAE number: 30650420.4.1001.0008. Next, hiPSC-CMs were washed with PBS 1X and
181 incubated with the secondary antibodies diluted in blocking solution: goat anti-Human Alexa
182 Fluor 647 (1:400; A-21445 - Invitrogen), goat anti-Rabbit Alexa Fluor 546 and goat anti-Mouse
183 Alexa Fluor 488 (1:400; A-11001 - Invitrogen) for 1 h at room temperature. Actin filaments were
184 stained with Alexa Fluor 568 phalloidin (1:10; A-12380 - Life Technologies) for 1 h. Nuclei
185 were stained with 300 nM 4′-6-diamino-2-phenylindole (DAPI) for 5 minutes and each well was
186 mounted with 50% PBS-Glycerol.
187
188 For quantitative analysis, images were acquired using Operetta® High-Content Screening System
189 (Perkin Elmer) with a 20x long working distance (WD) objective lens from at least 10 fields per
190 well. For cell surface area measurement, images of F-actin stained cardiomyocytes were
191 segmented using Cellpose and the area was measured using NIH ImageJ software (Stringer et al.,
192 2021). For the other analyses, data were evaluated using the Columbus™ Image Data Storage
193 and Analysis System (Perkin Elmer) for image segmentation and object detection. Fluorescence
194 threshold was set to determine positive and negative cells for each marker. Representative
195 immunostaining images were acquired on a Leica TCS-SP8 confocal microscope using a 63x oil-
196 immersion objective lens.
197
198

199   Measurements of Cell Death and Cytokines
200   Monolayers of hiPSC-CMs in 96-well plates (70-90% confluence) were treated with various
201   concentrations of NE-100. The neutral red assay was performed, and viability was estimated by
202   the percentage relative to untreated condition (vehicle) using the mean of 6 technical replicates
203   per experiment.
204
205   The levels of IL-6, IL-8, and TNF-α were quantified in the supernatants from uninfected and
206   SARS-CoV-2-infected hiPSC-CMs by ELISA (R&D Systems), following manufacturer's
207   instructions. Control groups (mock and cells infected with SARS-CoV-2 only) were also
208   analyzed in Aragão et al., 2021. The results were obtained as picograms per milliliter (pg/ml) and
209   are expressed as fold-change relative to untreated uninfected control. Cell death was determined
210   according to the activity of lactate dehydrogenase (LDH) in the culture supernatants using a
211   CytoTox® Kit (Promega, USA) according to the manufacturer's instructions. Supernatants were
212   centrifuged at 5,000 rpm for 1 minute, to remove cellular debris.
213
214   Gene Expression Analysis
215   Total RNA was isolated using TRIzol, according to the manufacturer's recommendations
216   (Thermo Fisher Scientific) and digested using DNase I, Amplification Grade (Invitrogen),
217   following the manufacturer's instructions. DNase-treated RNA samples (1 μg) were converted to
218   complementary DNA (cDNA) using the M-MLV enzyme (Thermo Fisher Scientific). Qualitative
219   endpoint PCR reactions were executed with the following primer sequences: S1R (forward 5'-
220   AGTAGGACCATGCACTCACACC-3'; reverse: 5'- CCCCATCCTTAACTCTAGAACC-3').
221   Glyceraldehyde-3-phosphate Dehydrogenase (GAPDH; forward: 5'-
222   TTCGACAGTCAGCCGCATC-3'; reverse: 5'-GACTCCACGACGTACTCAGC-3') was used
223   as the endogenous housekeeping control gene. Each PCR reaction was performed in a 10 μL
224   mixture containing 0.25 U GoTaq G2 Hot Start Polymerase (Promega), 1x GoTaq G2 Buffer, 1.5
225   mM MgCl2 (Invitrogen), 200 nM of each primer (forward and reverse), 200 μM dNTP mixture
226   containing the four deoxyribonucleotides (dATP, dCTP, dTTP, and dGTP), and 10 ng of cDNA
227   template. Appropriate negative controls and genomic DNA positive controls were incorporated
228   into each experiment. Amplification thermal program included an initial denaturation step of
229   95°C for 3 min and 40 cycles of 95°C for 15 s, 58°C for 15 s and 72°C for 15 s using the
230   ProFlex™ PCR System Thermal Cycler (Applied Biosystems). Subsequently, total amount of
231   PCR product was separated by electrophoresis at 120 V for 30 min in 2% agarose gel diluted in
232   1X Tris-acetate EDTA buffer (w/v) and stained with 0.01% of SYBR Safe (Thermo Fisher).
233   For real-time quantitative PCR, the reactions were conducted in three replicates with a final
234   volume of 10 μL containing 1X GoTaq qPCR Master Mix (Promega), 300 nM CXR Reference
235   Dye, 200nM of each SYBR green designed primers: Angiotensin I Converting Enzyme 2
236   (ACE2; forward: 5'-CGAAGCCGAAGACCTGTTCTA-3'; reverse: 5'-
237   GGGCAAGTGTGGACTGTTCC-3'); Natriuretic Peptide A (ANP; forward: 5'-
238   CAACGCAGACCTGATGGATTT-3'; reverse: 5'-AGCCCCGCTTCTTCATTC-3'); Spliced

239 X-Box Binding Protein 1 (sXBP1; forward: 5'- CTGAGTCCGAATCAGGTGCAG-3'; reverse:
240 5'-ATCCATGGGGAGATGTTCTGG-3'); Unspliced X-Box Binding Protein 1 (usXBP1;
241 forward: 5'-CAGCACTCAGACTACGTGCA-3'; reverse: 5'-
242 ATCCATGGGGAGATGTTCTGG-3'); Total X-Box Binding Protein 1 (totalXBP1; forward: 5'-
243 TGGCCGGGTCTGCTGAGTCCG-3'; reverse: 5'-ATCCATGGGGAGATGTTCTGG-3');
244 C/EBP-homologous protein (CHOP; forward: 5'-AGAACCAGGAAACGGAAACAGA-3';
245 reverse: 5'-TCTCCTTCATGCGCTGCTTT-3'); Actinin Alpha 1 (ACTN1; forward: 5'-
246 CCCGAGCTGATTGACTACGG-3'; reverse: 5'-GCAGTTCCAACGATGTCTTCG-3');
247 Actinin Alpha 2 (ACTN2; forward: 5'-GACATCGTGAACACCCCTAAAC-3'; reverse: 5'-
248 CCGCAAAAGCGTGGTAGAA); Actin Alpha 1 (ACTA1; forward: 5'-
249 TGCCAACAACGTCATGTCG-3'; reverse: 5'-CAGCGCGGTGATCTCTTTCT-3'); Troponin
250 I3, Cardiac Type (TNNI3; forward: 5'-TTTGACCTTCGAGGCAAGTTT-3'; reverse: 5'-
251 CCCGGTTTTCCTTCTCGGTG-3'); Troponin I1, Slow Skeletal Type (TNNT1; forward: 5'-
252 TGATCCCGCCAAAGATCCC-3'; reverse: 5'-TCTTCCGCTGCTCGAAATGTA-3'); Myosin
253 Heavy Chain 6 (MYH6; forward: 5'- GCCCTTTGACATTCGCACTG-3'; reverse: 5'-
254 GGTTTCAGCAATGACCTTGCC-3'); Myosin Heavy Chain 7 (MYH7; forward: 5'-
255 TCACCAACAACCCCTACGATT-3'; reverse: 5'- CTCCTCAGCGTCATCAATGGA-3'); and
256 10 ng of cDNA per reaction. The reactions were performed on a StepOnePlus ™ Real-Time PCR
257 System thermocycler (Applied Biosystems). The relative expression of the genes of interest
258 (GOI) was normalized by endogenous control genes: Glyceraldehyde-3-phosphate
259 Dehydrogenase (GAPDH; forward: 5'-GCCCTCAACGACCACTTTG-3'; reverse: 5'-
260 CCACCACCCTGTTGCTGTAG-3') and Hypoxanthine Phosphoribosyl transferase 1 (HPRT-1;
261 forward 5'-CGTCGTGATTAGTGATGATGAACC-3'; reverse: 5'-
262 AGAGGGCTACAATGTGATGGC-3').
263
264 Data analysis was performed with the N_0 method implemented in LinRegPCR v. 2020.0
265 software, which considers efficiency estimated by the window-of-linearity method, as proposed
266 by Ramakers et al. (2003) and Ruijter et al. (2009) (Ramakers et al., 2003; Ruijter et al., 2009).
267 N_0 values were calculated using default parameters and the arithmetic mean of N_0 values from
268 GOI were normalized by taking its ratio to the N_0 of the geometric mean of the endogenous
269 control genes (REF) GAPDH and HRRT-1 (N_0GOI /N_0REF).
270
271 Protein Expression
272 Media was completely removed from hiPSC-CMs, and 40μL of sample buffer without
273 bromophenol blue (62.5 mM Tris-HCl, pH 6.8, containing 10% glycerol, 2% SDS, and 5% 2-
274 mercaptoethanol) was added to each well. Next, cell extracts were boiled at 95°C for 5 min,
275 centrifuged 16,000 x g for 15 min at 4°C, and the supernatant was collected. Protein content was
276 estimated using the Bio-Rad Protein Assay (#5000006, Bio-Rad). After the addition of
277 bromophenol blue (0.02%), samples were separated by electrophoresis on an 8% SDS
278 polyacrylamide gel and transferred to polyvinylidene difluoride (PVDF) membranes.

279 Western blotting was carried out with minor modification from the described (Towbin, Gordon
280 & Staehelin, 1989). Briefly, membranes were blocked in 5% non-fat milk diluted in Tris-
281 Buffered Saline with 0.1% Tween-20 (TBS-T) for 1 h at room temperature. Membranes were
282 then incubated overnight at 4°C with primary antibodies diluted in TBS-T with 5% non-fat milk.
283 Then, membranes were washed and incubated with peroxidase-conjugated antibodies. The
284 signals were developed using ECL Prime Western Blotting System (#GERPN2232, Sigma) for 5
285 minutes and chemiluminescence was detected with an Odyssey-FC System®□ (LI-COR
286 Biosciences).
287
288 Stripping protocol was performed to break bonds between the antibodies and the transferred
289 proteins in order to reuse membranes. Briefly, membranes were incubated for three cycles of 10
290 minutes in a stripping buffer (pH 2.2, 200 mM glycine, SDS 0.1% and 1% Tween-20). Then, the
291 buffer was discarded, the membranes were washed for 5 minutes with PBS and 5 minutes with
292 0.1% TBS-T (three times each). Next, membranes were blocked again and proceeded with the
293 above-described steps. Full-length membranes are displayed in Supplemental Figure 5.
294
295 Beating Frequency Evaluation
296 hiPSC-CMs were plated on 96-well plates (1.8×10^4 cells per well) and treated with NE-100 1μM
297 or vehicle (DMSO) before incubating at 37ºC. At 24- and 48-hours post-treatment, beating
298 frequency was measured by manually counting the synchronous contractions of the monolayer
299 for 60 seconds (beats per minute). Cells were observed using an EVOS cell imaging system
300 (Thermo Fisher Scientific), in brightfield mode. Representative videos were recorded using
301 Operetta® High-Content Screening System (Perkin Elmer) for each condition at baseline and 48
302 h after treatment with vehicle or NE-100.
303
304 Statistical Analysis
305 Data are presented as mean values, and error bars indicate the standard error of the mean
306 (S.E.M). Statistical differences were analyzed using nested t-test, unpaired two-tailed Welch's t-
307 test and between three or more groups, unpaired multiple t-tests (Holm-Sidak method) or
308 ordinary one-way ANOVA with Holm-Sidak post-hoc. Prism v8.0 (GraphPad) was used for data
309 analysis and graphics, where statistical significance was accepted at P<0.05. The tests and p
310 values are specified in figure legends and the symbols represent $p < 0.05$, **$p < 0.01$, *$p < 0.001$,
311 ***$p < 0.0001$.
312

313 **Results**
314 **Human induced pluripotent stem cell-derived cardiomyocytes (hiPSC-CMs) express the**
315 **Sigma-1 receptor (S1R)**
316 Human cardiomyocytes were differentiated from induced pluripotent stem cells according to
317 established protocols (Cruvinel et al., 2020). Differentiation to cardiomyocytes resulted in low
318 expression of the pluripotency marker OCT-4 (0.8% ± 0.4%) and high expression of the specific

319 cardiac muscle marker troponin T (cTnT) (88.4% ± 8.4%) (Supplemental Figure 1 A). The
320 presence of cTnT was confirmed by immunostaining, as was cell morphology with F-actin
321 staining (Supplemental Figure 1 B).
322
323 Previous studies showed that S1R was expressed in the human heart tissue and in atrial and
324 ventricular cardiomyocytes of rodents (Novakova et al., 1995, 2010; Fagerberg et al., 2014;
325 Abdullah et al., 2020). Here, we showed S1R mRNA and protein in hiPSC-CMs (Figure 1 A and
326 B, respectively). Immunostaining showed that S1R is in the nuclei and in the perinuclear region
327 of the cells (Figure 1 C). This is consistent with previous findings of the distribution of S1R in
328 cells from rodents and yeasts and in human cell lines (Dussossoy et al., 1999; Hayashi & Su,
329 2003a). S1R is enriched at the mitochondria-associated ER membrane (MAM) (Hayashi & Su,
330 2007; Morales-Lázaro, González-Ramírez & Rosenbaum, 2019). We found that part of cytosolic
331 S1R staining was in close apposition with the mitochondrial marker VDAC1/Porin (Figure 1 D)
332 and with the ER chaperone lectin Calnexin (CNX) (Figure 1 E) in hiPSC-CMs.
333
334 **Inhibition of S1R reduces infection and replication of SARS-CoV-2 and prevents cell death**
335 **in human cardiomyocytes**
336 To test whether S1R had a direct influence on SARS-CoV-2 infection in human cardiomyocytes,
337 the selective S1R antagonist, NE-100, was used to inhibit this receptor in hiPSC-CMs prior to
338 exposure to the virus. NE-100 has a binding affinity for S1R within the nanomolar range and an
339 IC50 200 times higher for other receptors, such as dopamine, serotonin, and phencyclidine
340 receptors (Okuyama et al., 1993). Exposure of cardiomyocytes to NE-100 in the micromolar
341 range for 24 h was reported to abolish the effects of a S1R agonist, similarly to what was
342 observed using small interference RNA (siRNA) (Tagashira et al., 2013). Then, following 24 h
343 exposure to 1 μM NE-100, hiPSC-CMs were infected with SARS-CoV-2 at the multiplicity of
344 infection (MOI) 0.1. Immunofluorescence using convalescent serum (CS) from a recovered
345 COVID-19 patient showed that 57.3% (± 11.1%) of cells were infected at 48 h.p.i (hours post-
346 infection) (Figure 2 A). CS-staining was confirmed with co-localization with the specific SARS-
347 CoV-2 Spike Protein (SP) (Supplemental Figure 2).
348
349 Importantly, the inhibition of S1R reduced the percentage of infected hiPSC-CMs to 35.8% (±
350 2.5%) (Figure 2 A and B). Moreover, whereas infection of hiPSC-CMs with SARS-CoV-2 led to
351 the production of infectious virions measured in the plaque assay, exposure to NE-100
352 considerably diminished this viral yield, with an average reduction of 82% plaque forming units
353 (PFU) at 48 h.p.i (Figure 2 C). SARS-CoV-2 infection was previously shown to induce
354 cytopathic features in hiPSC-CMs, mostly related to myofibrillar disruption, as described by
355 other groups (Perez-Bermejo et al., 2021; Marchiano et al., 2021). Likewise, we detected a
356 pattern of structural disarrangement of cardiac troponin T staining, as shown in Supplemental
357 Figure 3.
358

359   The release of lactate dehydrogenase (LDH) confirmed that SARS-CoV-2 caused cardiomyocyte
360   death, as previously reported (Sharma et al., 2020). At 24, 48, and 72 h.p.i, LDH was elevated by
361   2.3, 5.6 and 2.7-fold, respectively, in SARS-CoV-2-infected cells when compared to controls
362   (Figure 2 D). NE-100 was able to decrease the release of LDH at 48 h.p.i and also tended to
363   decrease cytotoxicity at 72 h.p.i (Figure 2 D). There was no increase in the release of LDH when
364   comparing uninfected to NE-100 treated controls (Figure 2 D). These results suggest that the
365   inhibition of S1R does not induce cell death and may protect hiPSC-CMs by decreasing
366   infection.
367
368   S1R is engaged in ER protein synthesis and acts as a chaperone for proteins translocating to cell
369   surface (Vela, 2020). We investigated whether the inhibition of S1R could be related to
370   modifications in the host cell receptor for viral entry, since it partially prevented the infection.
371   The expression of the main viral entry receptor, ACE2, was measured after 24 h exposure to 1
372   µM NE-100. There was a reduction in the levels of ACE2 mRNA, albeit not statistically
373   significant (p=0.0790) (Supplemental Figure 4 A). However, western blot analysis of ACE2
374   after NE-100 treatment did not show differences at the protein level (Supplemental Figure 4, B
375   and C). These data suggest that the inhibition of SARS-CoV-2 infection in hiPSC-CMs can
376   occur through mechanisms other than a reduction in the availability of ACE2 under the above-
377   described conditions.
378
379   **NE-100 attenuates cytokine release by SARS-CoV-2 infected hiPSC-CMs**
380   Cell death is the final denouement of hiPSC-CMs at 72 h.p.i (Sharma et al., 2020; Aragão et al.,
381   2021). To investigate events before cell death, we analyzed some cytokines associated with
382   COVID-19 at 24 and 48 h.p.i. This strategy was previously shown to be significant in the context
383   of the infection of hiPSC-CMs by other pathogens that target the heart (Bozzi et al., 2019).
384
385   SARS-CoV-2 infection increased the release of interleukin (IL)-6 when compared to control.
386   NE-100 decreased this response at 24 h.p.i and 48 h.p.i (Figure 3 A and 3 B). Conversely, no
387   differences in the secretion of IL-8 were observed at 24 h.p.i (Figure 3 A), however, at 48 h.p.i,
388   SARS-CoV-2 increased IL-8 by 5.5-fold relative to the mock condition (Figure 3 B).
389   Comparably to the modulation of IL-6, NE-100 decreased the secretion of IL-8 (Figure 3 B).
390   Tumor necrosis factor-alpha (TNF-α) levels were only transiently increased at 24 h.p.i (3.3-fold)
391   but were nevertheless inhibited by previous NE-100 treatment (Figure 3 and B).
392
393   **S1R inhibition decreases beating in cardiomyocytes**
394   To investigate the consequences of the inhibition of S1R in human cardiomyocytes by itself, we
395   conducted further tests on the effects of NE-100 in hiPSC-CMs. We first analyzed whether NE-
396   100 induces cell death. NE-100 does not decrease cell viability after 72 h at concentrations
397   ranging from 10 nM to 10 µM as measured by the neutral red assay (Figure 4 A). Also, hiPSC-
398   CMs treated with 1 µM NE-100 for 48 h showed no changes in the number of pyknotic nuclei,

399   which represents an irreversible chromatin-condensed nuclear state characteristic of cell death
400   (Figure 4 B).

401

402   Furthermore, given that S1R function is important for the ER stress response, we investigated
403   whether NE-100 modulates the endonuclease activity of inositol-requiring enzyme 1α (IRE1α)
404   by analysis of splicing of XBP1 mRNA, measuring the levels of spliced XBP1 mRNA (sXBP1),
405   in addition to the unspliced (uXBP1) and total XBP1 mRNAs (Oslowski & Urano, 2011). We
406   found low levels of sXBP1 mRNA and high levels of uXBP1 mRNA in hiPSC-CMs which are
407   consistent with cells under non-ER stress condition (Figure 4 C). NE-100 treatment did not
408   affect levels of sXBP1 or uXBP1 mRNAs/total XBP1 (Figure 4 C). These results indicate that
409   NE-100 did not induce activation of IRE1α in hiPSC-CMs under these conditions. Another
410   indicator of ER stress response is the upregulation of the C/EBP-homologous protein (CHOP or
411   GADD153). Again, we did not find changes in CHOP mRNA after NE-100 treatment (Figure 4
412   D).

413

414   These data suggest that NE-100 does not induce hiPSC-CMs death or ER stress response in the
415   absence of additional stressor stimuli. However, one of the main functional features displayed by
416   cultured cardiomyocytes is their ability to perform spontaneous contractions. In that matter,
417   hiPSC-CMs are suitable to evaluate drug-induced changes in contractility (Pointon et al., 2015;
418   Niehoff et al., 2019). We observed a decrease from 17.7 (± 5.9) beats per minute (bpm) to 6.7 (±
419   1.8) bpm and from 14.7 (± 2.8) bpm to 4.1 (± 0.8) bpm after 24 h and 48 h of NE-100 exposure,
420   respectively (Figure 4 E and Supplemental Videos S1-S4). These results suggest that the
421   inhibition of S1R leads to changes in beating rate and a putative deviation in contractility.

422

423   **The S1R antagonist NE-100 induces maladaptive transcriptional and structural changes in**
424   **human cardiomyocytes**
425   The findings on the decremental impact of NE-100 on the cardiomyocytes beating rate led us to
426   pursue this issue further. S1R plays a cardioprotective role during maladaptive cardiac
427   remodeling and the anti-hypertrophic properties of S1R agonists have been described (Tagashira
428   & Fukunaga, 2012; Tagashira et al., 2013; Hirano, Tagashira & Fukunaga, 2014). Therefore, we
429   also investigated if the S1R antagonist NE-100 alone could induce a hypertrophic response. To
430   that end, we quantified the expression of key genes upon S1R inhibition. First, by measuring
431   mRNA levels of the atrial natriuretic peptide (ANP), which is one of the main transcripts of the
432   fetal program for cardiac growth. ANP overexpression is frequently correlated to cardiac
433   hypertrophy but NE-100 decreased ANP mRNA expression by 1.49-fold after 24 h (Figure 5 A).
434   There was also no increase in the average cell surface area of hiPSC-CMs observed by F-actin
435   staining. In fact, more like the contrary, NE-100 exposure caused a decrease in the average cell
436   surface area after 48 h (Figure 5 B), which is a phenotype opposite to the expected for
437   cardiomyocyte hypertrophic responses *in vitro* (Watkins et al., 2012).

438   After observing cell shrinking in longer exposures to NE-100, we then hypothesized that S1R
439   inhibition could be triggering morphological changes. Hence, we investigated the expression of
440   myofibril-associated genes important for cytoarchitecture maintenance and observed a
441   downregulation of 4 out of 7 genes investigated. The decreased expression of *ACTN2* (- 1.53-
442   fold), *ACTA1* (- 11.1-fold), *TNNI3* (- 2.32-fold) and *TNNT1* (- 2.43-fold) after the inhibition of
443   S1R suggests a transcriptional regulation that could impair sarcomeric organization and
444   cardiomyocyte cytoskeletal integrity (Figure 5 C). *ACTN1* and *MYH7* expression did not show
445   significant changes upon NE-100 exposure (Figure 5 C). Interestingly, *MYH7* upregulation is
446   highly associated with hypertrophy (Krenz & Robbins, 2004; Gupta, 2007). Therefore, this result
447   corroborates the assumption that the inhibition of S1R in the absence of a hypertrophic stimulus
448   is not sufficient to activate the molecular profile of cardiac hypertrophy in hiPSC-CMs (i.e., *ANP*
449   and *MYH7* upregulation). Intriguingly, *MYH6* was the only transcript upregulated by 3.44-fold
450   (p=0.0502) (Figure 5 C), which could represent a transcriptional compensatory adaptation.
451
452   Furthermore, cardiac troponin T (cTnT) staining analysis revealed a significant decrease both in
453   immunoreactive area and fluorescence intensity on hiPSC-CMs exposed to NE-100 when
454   compared to untreated controls (Figure 5 D and E, respectively). These results are probably
455   attributable also to a decrease in cellular cTnT content rather than exclusively to a change in the
456   cell area, indicating a considerable loss of troponin. Consistently, the morphology of cytoskeletal
457   fibers was grossly affected after 48 h, as shown in confocal fluorescence images (Figure 5 F).
458   Taken together, our results suggest that S1R inhibition caused neither change in cell viability nor
459   induction of hypertrophy parameters. However, despite this apparent lack of negative effects
460   related to cell death and hypertrophy, there was a downregulation of genes encoding structural
461   proteins and cytoskeletal impairment via a decrease in cardiac troponin T content. The latter
462   significant effects could explain in part the beating frequency reduction of human
463   cardiomyocytes exposed to NE-100.
464
465

466   **Discussion**
467   In this study, we show that hiPSC-CMs are permissive to productive infection of SARS-CoV-2,
468   corroborating previous reports (Bulfamante et al., 2020; Sharma et al., 2020; Choi et al., 2020;
469   Bojkova et al., 2020; Bailey et al., 2021; Perez-Bermejo et al., 2021; Marchiano et al., 2021).
470   Although the presence of SARS-CoV-2 in the postmortem heart is still controversial, the
471   cytopathic features following cardiomyocyte infection *in vitro* are similar to those observed in
472   the cardiac tissue of patients deceased from COVID-19, including sarcomeric fragmentation,
473   innate immune cells activation and cell death (Lindner et al., 2020; Bailey et al., 2021; Perez-
474   Bermejo et al., 2021). Here, we confirmed that SARS-CoV-2 induces cardiotoxicity by directly
475   infecting cardiomyocytes.
476

477   Aside from viral infection and replication, immune responses are a hallmark of COVID-19
478   pathology that can also be modeled using hiPSC-CMs (Azkur et al., 2020; Dariolli et al., 2021).
479   Along with monocytes and fibroblasts, cardiomyocytes are considered an important source of
480   cytokines during events such as heart failure (Aoyagi & Matsui, 2012). In fact, Wong and
481   collaborators have shown that SARS-CoV-2 upregulates the expression of pro-inflammatory
482   cytokines in hiPSC-CMs, including IL-6, IL-8, and TNF-α (Wong et al., 2020). Here, we
483   confirmed the release of cytokines after the infection with SARS-CoV-2. Elevated levels of IL-6
484   are correlated with cardiac damage and heart failure in rodent models (Janssen et al., 2005).
485   Moreover, previous reports demonstrated that IL-6 produced by cardiomyocytes promotes
486   inflammation in the heart by recruiting neutrophils (Youker et al., 1992). Interestingly, IL-8,
487   which was also increased, is a neutrophil chemotactic factor correlated with heart disease
488   (Rothenbacher et al., 2006; Akasaka et al., 2006). Myocardial infiltration of neutrophils has been
489   reported in the hearts of COVID-19 patients and is associated with myocardial damage (Yao et
490   al., 2020).
491
492   Nonetheless, the characterization of the interlinkage between the virus and intracellular
493   structures may provide therapeutic clues against COVID-19. A SARS-CoV-2–human protein
494   interaction map showed that NSP6 interacts directly with S1R (Gordon et al., 2020b). The
495   antiviral activity of sigma receptor ligands was described in Vero E6 cells (Gordon et al., 2020b).
496   S1R knockdown in A549 cells and S1R knockout in Caco-2 cells further confirmed S1R, but not
497   Sigma-2 receptor, as a host-dependency factor for SARS-CoV-2 infection (Gordon et al., 2020a).
498   NSP6 orchestrates vesicle trafficking and regulates ER remodeling during the replication of
499   mammalian coronaviruses (Cottam et al., 2011b) and its interaction with S1R possibly
500   contributes to the rearrangement of endomembrane compartments. S1R is critical for the
501   replication of Hepatitis C Virus (HCV) that occur inside ER, where this receptor is mostly
502   expressed (Ritzenthaler & Elamawi, 2006; Friesland et al., 2013). Interestingly, HCV is a
503   positive-sense single-stranded RNA virus. Altogether, these data support S1R as a host target to
504   dampen SARS-CoV-2 replication. On the other hand, the function of S1R in the homeostasis of
505   cardiac cells makes this receptor a target regarding cellular impairments. Also, since COVID-19
506   triggers cardiac dysfunctions, drugs with negative cardiac effects would be unfeasible as a
507   therapeutic approach (Wu et al., 2020; Magadum & Kishore, 2020). The inhibition of S1R could
508   be detrimental to cardiac physiology since this receptor is important for bioenergetics and
509   response to stress in heart cells (Shinoda et al., 2016a,b; Stracina & Novakova, 2018).
510
511   The inhibition of S1R with NE-100 reduced the number of infected cells, the replication of
512   SARS-CoV-2, prevented infection-associated cell death and attenuated the release of cytokines.
513   However, it is the activation of S1R that has been described with anti-inflammatory properties
514   (Szabo et al., 2014; Rosen et al., 2019; Zhou et al., 2019). It was recently reported that the S1R
515   agonist fluvoxamine prevents clinical deterioration of symptomatic COVID-19 and the
516   persistence of residual symptoms (Lenze et al., 2020; Seftel & Boulware, 2021). Consequently,

517   the reduction of pro-inflammatory cytokines described here is more likely due to the inhibition of
518   infection rather than a direct suppression of the release of cytokines.
519
520   Although S1R is foregrounded in COVID-19 research, it is currently unclear if a S1R antagonist
521   or agonist could be better to treat the disease, since in vitro reports show that S1R antagonists
522   prevent SARS-CoV-2 replication and S1R agonists have proviral activity, while clinical
523   evidence suggests that S1R agonists prevent worsening of symptoms. In spite of that, evidence of
524   side effects of S1R ligands, especially cardiac-specific detrimental cellular effects, are
525   overlooked in current studies and should be acknowledged for further treatment options. In order
526   to look into the consequences of S1R inhibition *per se* on hiPSC-CMs, other aspects were
527   investigated beyond antiviral activity. The survival of cardiomyocytes was not affected by NE-
528   100. Given the role of S1R in ER stress response, the mRNA levels of sXBP1 and CHOP were
529   investigated as another aspect of toxicity (Wang et al., 2018). The spliced XBP1 analysis
530   represents a reliable indirect method to determine IRE1α activation, which is one of the major
531   ER stress sensors involved in pro-inflammatory cytokine production (Oslowski & Urano, 2011;
532   Rosen et al., 2019).
533
534   Alam and collaborators' have demonstrated that the knockdown of S1R increases the expression
535   of CHOP in neonatal rat ventricular cardiomyocytes, while decreases spliced XBP1 with
536   tunicamycin (Alam et al., 2017). It means that S1R is crucial for coping with ER stress and that
537   its depletion favors cytotoxic ER stress response in cardiac cells by CHOP upregulation and
538   impaired sXBP1-mediated signaling. In the present study, no changes in the transcript levels of
539   sXBP1 and CHOP were detected in hiPSC-CMs with NE-100. Our results suggest that there is
540   no intrinsic ER stress induction by NE-100, but future studies should explore the role of S1R
541   ligands in ER stress transcripts' expression upon ER-stressor stimuli in hiPSC-CMs.
542
543   Nonetheless, we observed that inhibition of S1R reduced the frequency of cardiomyocytes'
544   beating. Consistent with our findings, it has been noted that S1R antagonists cause delayed
545   cardiac repolarization, impairment of rate adaptation, and increased risk for drug-induced
546   arrhythmia (Witchel, 2011; Balasuriya et al., 2014; Morales-Lázaro, González-Ramírez &
547   Rosenbaum, 2019). Interestingly, haloperidol, which is a S1R antagonist, reduces the replication
548   of SARS-CoV-2 (Gordon et al., 2020b,a). However, this antipsychotic did not decrease the risk
549   for intubation or death in hospitalized patients (Hoertel et al., 2021). The anti-SARS-CoV-2
550   activity of the broad-spectrum antiviral remdesivir was described in human cardiomyocytes by
551   Choi and colleagues, together with a safety profile evaluation that stipulated considerable
552   arrhythmogenic and cardiotoxic risk *in vitro*. These results, raised concerns regarding the drug-
553   induced cardiotoxicity of repositioned pre-approved compounds to manage COVID-19 (Choi et
554   al., 2020). The contractile capacity of cardiomyocytes is related to calcium availability. Since
555   S1R is a key regulator of intracellular calcium homeostasis, the possibility that blocking its
556   function may hamper the availability of cytoplasmic calcium and decrease beating rate in hiPSC-

557 CMs should be considered. Indeed, previous studies showed an interconnection among S1R and
558 mitochondrial function, calcium handling and contractility (Ela et al., 1994; Tarabová, Nováková
559 & Lacinová, 2009). Although there is abundant data on S1R-dependent modulation of calcium
560 homeostasis, ER stress response and hypertrophy (Bhuiyan & Fukunaga, 2009; Tagashira &
561 Fukunaga, 2012; Tagashira et al., 2013), no previous study explored the consequences of the
562 inhibition of S1R in the integrity of human cardiomyocytes' cytoskeleton.
563
564 S1R is a direct target of methamphetamine (Nguyen et al., 2005). Heart tissue from S1R
565 knockout mice and autopsy samples of human methamphetamine users present fibrosis and signs
566 of contractile dysfunction, suggesting a correlation between S1R and heart tissue remodeling
567 (Abdullah et al., 2018, 2020). Although S1R activation is known to protect cardiomyocytes from
568 hypertrophy upon pressure-overload, in the present study exposure of hiPSC-CMs to NE-100
569 with no secondary hypertrophic stimulus was not sufficient to neither increase the expression of
570 *ANP* and *MYH7* nor cellular size.
571
572 The association between S1R and sarcomeric integrity was hypothesized (Alam et al., 2017), but
573 morphological changes in human cardiomyocytes following S1R inhibition were not explored.
574 Herein, S1R inhibition compromised the morphology of hiPSC-CMs with a perturbation of
575 cytoskeletal architecture. The changes in morphology were accompanied by a decrease in cardiac
576 troponin T and preceded by a downregulation of genes encoding key cytoskeletal proteins in
577 cytoarchitecture maintenance, such as α-actinin 2, actin-α 1, troponin I3 and troponin T1.
578 Importantly, the downregulation of these genes is associated with cardiotoxicity induced by
579 doxorubicin, daunorubicin and mitoxantrone (Chaudhari et al., 2016). Out of seven targets
580 investigated, *MYH6* was the only transcript increased with NE-100. It was previously
581 demonstrated that the expression of myosin heavy chain is specifically induced as a
582 compensatory response following disruption of the myofibrillar structure in hiPSC-CMs (Perez-
583 Bermejo et al., 2021). Future studies should elucidate the mechanisms behind cytoskeletal
584 changes and cardiomyocyte recovery after inhibition of S1R.
585
586

Conclusions

588 The disruption of cytoskeletal and sarcomeric proteins by a decrease in expression or anomalous
589 arrangement could underlie cardiomyopathies and heart failure, representing a potential
590 mechanism by which drugs inhibiting S1R jeopardize cardiac integrity and contractility
591 (Sequeira et al., 2014). Our results suggest that the inhibition of S1R leads to morphological and
592 transcriptional changes in human cardiac cells and, therefore, its use as a therapeutic strategy
593 against COVID-19 should be further investigated before translated to clinical application, due to
594 the concern of drug-induced cardiac damage and malfunction.
595
596

Acknowledgements

We thank Professor Leticia Raposo for the support in the statistical analysis of the data presented in this manuscript. We also thank Emiliano Horacio Medei and Renata Junqueira Moll Bernardes for scientific discussions. This work was developed as part of the doctoral thesis of J.A.S. at the Morphological Sciences Program, Biomedical Sciences Institute, Federal University of Rio de Janeiro (UFRJ), Rio de Janeiro, Brazil.

References

Abdullah CS, Aishwarya R, Alam S, Morshed M, Remex NS, Nitu S, Kolluru GK, Traylor J, Miriyala S, Panchatcharam M, Hartman B, King J, Bhuiyan MAN, Chandran S, Woolard MD, Yu X, Goeders NE, Dominic P, Arnold CL, Stokes K, Kevil CG, Orr AW, Bhuiyan MS. 2020. Methamphetamine induces cardiomyopathy by Sigmar1 inhibition-dependent impairment of mitochondrial dynamics and function. *Communications Biology 2020 3:1* 3:1–20. DOI: 10.1038/s42003-020-01408-z.

Abdullah CS, Alam S, Aishwarya R, Miriyala S, Panchatcharam M, Bhuiyan MAN, Peretik JM, Orr AW, James J, Osinska H, Robbins J, Lorenz JN, Bhuiyan MS. 2018. Cardiac Dysfunction in the Sigma 1 Receptor Knockout Mouse Associated With Impaired Mitochondrial Dynamics and Bioenergetics. *Journal of the American Heart Association* 7. DOI: 10.1161/JAHA.118.009775.

Akasaka Y, Morimoto N, Ishikawa Y, Fujita K, Ito K, Kimura-Matsumoto M, Ishiguro S, Morita H, Kobayashi Y, Ishii T. 2006. Myocardial apoptosis associated with the expression of proinflammatory cytokines during the course of myocardial infarction. *Modern Pathology* 19:588–598. DOI: 10.1038/modpathol.3800568.

Alam S, Abdullah CS, Aishwarya R, Orr AW, Traylor J, Miriyala S, Panchatcharam M, Pattillo CB, Bhuiyan MS. 2017. Sigmar1 regulates endoplasmic reticulum stress-induced C/EBP-homologous protein expression in cardiomyocytes. *Bioscience Reports* 37:20170898. DOI: 10.1042/BSR20170898.

Aoyagi T, Matsui T. 2012. The Cardiomyocyte as a Source of Cytokines in Cardiac Injury. *Journal of Cell Science & Therapy* s5. DOI: 10.4172/2157-7013.s5-003.

Aragão LGHS, Oliveira JT, Temerozo JR, Mendes MA, Salerno JA, Pedrosa CSG, Puig-Pijuan T, Veríssimo CP, Ornelas IM, Torquato T, Vitória G, Sacramento CQ, Fintelman-Rodrigues N, Da Silva Gomes Dias S, Soares VC, Souza LRQ, Karmirian K, Goto-Silva L, Biagi D, Cruvinel EM, Dariolli R, Furtado DR, Bozza PT, Borges HL, Souza TML, Guimarães MZP, Rehen SK. 2021. WIN 55,212-2 shows anti-inflammatory and survival properties in human iPSC-derived cardiomyocytes infected with SARS-CoV-2. *PeerJ* 9. DOI: 10.7717/peerj.12262.

Azkur AK, Akdis M, Azkur D, Sokolowska M, van de Veen W, Brüggen MC, O'Mahony L, Gao Y, Nadeau K, Akdis CA. 2020. Immune response to SARS-CoV-2 and mechanisms of immunopathological changes in COVID-19. *Allergy: European Journal of Allergy and Clinical Immunology* 75:1564–1581. DOI: 10.1111/all.14364.

Bailey AL, Dmytrenko O, Greenberg L, Bredemeyer AL, Ma P, Liu J, Penna V, Winkler ES, Sviben S, Brooks E, Nair AP, Heck KA, Rali AS, Simpson L, Saririan M, Hobohm D, Stump WT, Fitzpatrick JA, Xie X, Zhang X, Shi P-Y, Hinson JT, Gi W-T, Schmidt C, Leuschner F, Lin C-Y, Diamond MS, Greenberg MJ, Lavine KJ. 2021. SARS-CoV-2 Infects Human Engineered Heart Tissues and Models COVID-19 Myocarditis. *JACC: Basic*

645   *to Translational Science*. DOI: 10.1016/j.jacbts.2021.01.002.
646   Balasuriya D, D'Sa L, Talker R, Dupuis E, Maurin F, Martin P, Borgese F, Soriani O,
647   Edwardson JM. 2014. A direct interaction between the sigma-1 receptor and the herg
648   voltage-gated K+ channel revealed by atomic force microscopy and homogeneous time-
649   resolved fluorescence (HTRF®). *Journal of Biological Chemistry* 289:32353–32363. DOI:
650   10.1074/jbc.M114.603506.
651   Bhuiyan MS, Fukunaga K. 2009. Stimulation of Sigma-1 receptor signaling by
652   dehydroepiandrosterone ameliorates pressure overload-induced hypertrophy and
653   dysfunctions in ovariectomized rats. *Expert Opinion on Therapeutic Targets* 13:1253–1265.
654   DOI: 10.1517/14728220903264064.
655   Bojkova D, Wagner JUG, Shumliakivska M, Aslan GS, Saleem U, Hansen A, Luxán G, Günther
656   S, Pham MD, Krishnan J, Harter PN, Ermel UH, Frangakis AS, Milting H, Zeiher AM,
657   Klingel K, Cinatl J, Dendorfer A, Eschenhagen T, Tschöpe C, Ciesek S, Dimmeler S. 2020.
658   SARS-CoV-2 infects and induces cytotoxic effects in human cardiomyocytes.
659   *Cardiovascular research* 116:2207–2215. DOI: 10.1093/cvr/cvaa267.
660   Bozzi A, Sayed N, Matsa E, Sass G, Neofytou E, Clemons K, Correa-Oliveira R, Stevens D, Wu
661   J. 2019. Using Human Induced Pluripotent Stem Cell-Derived Cardiomyocytes as a Model
662   to Study Trypanosoma cruzi Infection. *Stem cell reports* 12:1232–1241. DOI:
663   10.1016/J.STEMCR.2019.04.017.
664   Brune S, Pricl S, Wünsch B. 2013. Structure of the σ1 receptor and its ligand binding site.
665   *Journal of Medicinal Chemistry* 56:9809–9819. DOI: 10.1021/jm400660u.
666   Bulfamante G Pietro, Perrucci GL, Falleni M, Sommariva E, Tosi D, Martinelli C, Songia P,
667   Poggio P, Carugo S, Pompilio G. 2020. Evidence of sars-cov-2 transcriptional activity in
668   cardiomyocytes of covid-19 patients without clinical signs of cardiac involvement.
669   *Biomedicines* 8:1–13. DOI: 10.3390/biomedicines8120626.
670   Chaudhari U, Nemade H, Wagh V, Gaspar JA, Ellis JK, Srinivasan SP, Spitkovski D, Nguemo
671   F, Louisse J, Bremer S, Hescheler J, Keun HC, Hengstler JG, Sachinidis A. 2016.
672   Identification of genomic biomarkers for anthracycline-induced cardiotoxicity in human
673   iPSC-derived cardiomyocytes: an in vitro repeated exposure toxicity approach for safety
674   assessment. *Archives of Toxicology* 90:2763–2777. DOI: 10.1007/s00204-015-1623-5.
675   Chen CY, Wang FL, Lin CC. 2006. Chronic hydroxychloroquine use associated with QT
676   prolongation and refractory ventricular arrhythmia. *Clinical Toxicology* 44:173–175. DOI:
677   10.1080/15563650500514558.
678   Choi SW, Shin JS, Park S-J, Jung E, Park Y-G, Lee J, Kim SJ, Park H-J, Lee J-H, Park S-M,
679   Moon S-H, Ban K, Go YY. 2020. Antiviral activity and safety of remdesivir against SARS-
680   CoV-2 infection in human pluripotent stem cell-derived cardiomyocytes. *Antiviral*
681   *Research*:104955. DOI: 10.1016/j.antiviral.2020.104955.
682   Cottam EM, Maier HJ, Manifava M, Vaux LC, Chandra-Schoenfelder P, Gerner W, Britton P,
683   Ktistakis NT, Wileman T. 2011a. Coronavirus nsp6 proteins generate autophagosomes from
684   the endoplasmic reticulum via an omegasome intermediate. *Autophagy* 7:1335–1347. DOI:
685   10.4161/auto.7.11.16642.
686   Cottam EM, Maier HJ, Manifava M, Vaux LC, Chandra-Schoenfelder P, Gerner W, Britton P,
687   Ktistakis NT, Wileman T. 2011b. Coronavirus nsp6 proteins generate autophagosomes from
688   the endoplasmic reticulum via an omegasome intermediate. *Autophagy* 7:1335–1347. DOI:
689   10.4161/auto.7.11.16642.
690   Cottam E, Whelband M, Wileman T. 2014. Coronavirus NSP6 restricts autophagosome

691   expansion. *Autophagy* 10:1426–1441. DOI: 10.4161/AUTO.29309.

692   Cruvinel E, Ogusuku I, Cerioni R, Rodrigues S, Gonçalves J, Góes ME, Alvim JM, Silva AC,
693   Lino V de S, Boccardo E, Goulart E, Pereira A, Dariolli R, Valadares M, Biagi D. 2020.
694   Long-term single-cell passaging of human iPSC fully supports pluripotency and high-
695   efficient trilineage differentiation capacity. *SAGE Open Medicine* 8:205031212096645.
696   DOI: 10.1177/2050312120966456.

697   Dariolli R, Campana C, Gutierrez A, Sobie EA. 2021. In vitro and in silico models to study
698   SARS-CoV-2 infection: integrating experimental and computational tools to mimic
699   "COVID-19 cardiomyocyte" *Frontiers in Physiology* 12:119. DOI:
700   10.3389/FPHYS.2021.624185.

701   Dussossoy D, Carayon P, Belugou S, Feraut D, Bord A, Goubet C, Roque C, Vidal H, Combes
702   T, Loison G, Casellas P. 1999. Colocalization of sterol isomerase and sigma(1) receptor at
703   endoplasmic reticulum and nuclear envelope level. *European journal of biochemistry*
704   263:377–386. DOI: 10.1046/J.1432-1327.1999.00500.X.

705   Ela C, Barg J, Vogel Z, Hasin Y, Eilam Y. 1994. Sigma receptor ligands modulate contractility,
706   Ca++ influx and beating rate in cultured cardiac myocytes. *Journal of Pharmacology and*
707   *Experimental Therapeutics* 269:1300–1309.

708   Fagerberg L, Hallstrom BM, Oksvold P, Kampf C, Djureinovic D, Odeberg J, Habuka M,
709   Tahmasebpoor S, Danielsson A, Edlund K, Asplund A, Sjostedt E, Lundberg E, Szigyarto
710   CAK, Skogs M, Ottosson Takanen J, Berling H, Tegel H, Mulder J, Nilsson P, Schwenk
711   JM, Lindskog C, Danielsson F, Mardinoglu A, Sivertsson A, Von Feilitzen K, Forsberg M,
712   Zwahlen M, Olsson I, Navani S, Huss M, Nielsen J, Ponten F, Uhlen M. 2014. Analysis of
713   the human tissue-specific expression by genome-wide integration of transcriptomics and
714   antibody-based proteomics. *Molecular and Cellular Proteomics* 13:397–406. DOI:
715   10.1074/mcp.M113.035600.

716   Friesland M, Mingorance L, Chung J, Chisari F V., Gastaminza P. 2013. Sigma-1 Receptor
717   Regulates Early Steps of Viral RNA Replication at the Onset of Hepatitis C Virus Infection.
718   *Journal of Virology* 87:6377–6390. DOI: 10.1128/jvi.03557-12.

719   Gnecchi M, Moretti F, Bassi EM, Leonardi S, Totaro R, Perotti L, Zuccaro V, Perlini S, Preda L,
720   Baldanti F, Bruno R, Visconti LO. 2020. Myocarditis in a 16-year-old boy positive for
721   SARS-CoV-2. *The Lancet* 395:e116. DOI: 10.1016/S0140-6736(20)31307-6.

722   Gordon DE, Hiatt J, Bouhaddou M, Rezelj V V., Ulferts S, Braberg H, Jureka AS, Obernier K,
723   Guo JZ, Batra J, Kaake RM, Weckstein AR, Owens TW, Gupta M, Pourmal S, Titus EW,
724   Cakir M, Soucheray M, McGregor M, Cakir Z, Jang G, O'Meara MJ, Tummino TA, Zhang
725   Z, Foussard H, Rojc A, Zhou Y, Kuchenov D, Hüttenhain R, Xu J, Eckhardt M, Swaney
726   DL, Fabius JM, Ummadi M, Tutuncuoglu B, Rathore U, Modak M, Haas P, Haas KM,
727   Naing ZZC, Pulido EH, Shi Y, Barrio-Hernandez I, Memon D, Petsalaki E, Dunham A,
728   Marrero MC, Burke D, Koh C, Vallet T, Silvas JA, Azumaya CM, Billesbølle C, Brilot AF,
729   Campbell MG, Diallo A, Dickinson MS, Diwanji D, Herrera N, Hoppe N, Kratochvil HT,
730   Liu Y, Merz GE, Moritz M, Nguyen HC, Nowotny C, Puchades C, Rizo AN, Schulze-
731   Gahmen U, Smith AM, Sun M, Young ID, Zhao J, Asarnow D, Biel J, Bowen A, Braxton
732   JR, Chen J, Chio CM, Chio US, Deshpande I, Doan L, Faust B, Flores S, Jin M, Kim K,
733   Lam VL, Li F, Li J, Li YL, Li Y, Liu X, Lo M, Lopez KE, Melo AA, Moss FR, Nguyen P,
734   Paulino J, Pawar KI, Peters JK, Pospiech TH, Safari M, Sangwan S, Schaefer K, Thomas P
735   V., Thwin AC, Trenker R, Tse E, Tsui TKM, Wang F, Whitis N, Yu Z, Zhang K, Zhang Y,
736   Zhou F, Saltzberg D, Hodder AJ, Shun-Shion AS, Williams DM, White KM, Rosales R,

737   Kehrer T, Miorin L, Moreno E, Patel AH, Rihn S, Khalid MM, Vallejo-Gracia A, Fozouni
738   P, Simoneau CR, Roth TL, Wu D, Karim MA, Ghoussaini M, Dunham I, Berardi F,
739   Weigang S, Chazal M, Park J, Logue J, McGrath M, Weston S, Haupt R, Hastie CJ, Elliott
740   M, Brown F, Burness KA, Reid E, Dorward M, Johnson C, Wilkinson SG, Geyer A, Giesel
741   DM, Baillie C, Raggett S, Leech H, Toth R, Goodman N, Keough KC, Lind AL, Klesh RJ,
742   Hemphill KR, Carlson-Stevermer J, Oki J, Holden K, Maures T, Pollard KS, Sali A, Agard
743   DA, Cheng Y, Fraser JS, Frost A, Jura N, Kortemme T, Manglik A, Southworth DR, Stroud
744   RM, Alessi DR, Davies P, Frieman MB, Ideker T, Abate C, Jouvenet N, Kochs G, Shoichet
745   B, Ott M, Palmarini M, Shokat KM, García-Sastre A, Rassen JA, Grosse R, Rosenberg OS,
746   Verba KA, Basler CF, Vignuzzi M, Peden AA, Beltrao P, Krogan NJ. 2020a. Comparative
747   host-coronavirus protein interaction networks reveal pan-viral disease mechanisms. *Science*
748   370. DOI: 10.1126/science.abe9403.
749 Gordon DE, Jang GM, Bouhaddou M, Xu J, Obernier K, White KM, O'Meara MJ, Rezelj V V.,
750   Guo JZ, Swaney DL, Tummino TA, Hüttenhain R, Kaake RM, Richards AL, Tutuncuoglu
751   B, Foussard H, Batra J, Haas K, Modak M, Kim M, Haas P, Polacco BJ, Braberg H, Fabius
752   JM, Eckhardt M, Soucheray M, Bennett MJ, Cakir M, McGregor MJ, Li Q, Meyer B,
753   Roesch F, Vallet T, Mac Kain A, Miorin L, Moreno E, Naing ZZC, Zhou Y, Peng S, Shi Y,
754   Zhang Z, Shen W, Kirby IT, Melnyk JE, Chorba JS, Lou K, Dai SA, Barrio-Hernandez I,
755   Memon D, Hernandez-Armenta C, Lyu J, Mathy CJP, Perica T, Pilla KB, Ganesan SJ,
756   Saltzberg DJ, Rakesh R, Liu X, Rosenthal SB, Calviello L, Venkataramanan S, Liboy-Lugo
757   J, Lin Y, Huang XP, Liu YF, Wankowicz SA, Bohn M, Safari M, Ugur FS, Koh C, Savar
758   NS, Tran QD, Shengjuler D, Fletcher SJ, O'Neal MC, Cai Y, Chang JCJ, Broadhurst DJ,
759   Klippsten S, Sharp PP, Wenzell NA, Kuzuoglu-Ozturk D, Wang HY, Trenker R, Young
760   JM, Cavero DA, Hiatt J, Roth TL, Rathore U, Subramanian A, Noack J, Hubert M, Stroud
761   RM, Frankel AD, Rosenberg OS, Verba KA, Agard DA, Ott M, Emerman M, Jura N, von
762   Zastrow M, Verdin E, Ashworth A, Schwartz O, d'Enfert C, Mukherjee S, Jacobson M,
763   Malik HS, Fujimori DG, Ideker T, Craik CS, Floor SN, Fraser JS, Gross JD, Sali A, Roth
764   BL, Ruggero D, Taunton J, Kortemme T, Beltrao P, Vignuzzi M, García-Sastre A, Shokat
765   KM, Shoichet BK, Krogan NJ. 2020b. A SARS-CoV-2 protein interaction map reveals
766   targets for drug repurposing. *Nature* 583:459–468. DOI: 10.1038/s41586-020-2286-9.
767 Gupta MP. 2007. Factors controlling cardiac myosin-isoform shift during hypertrophy and heart
768   failure. *Journal of molecular and cellular cardiology* 43:388. DOI:
769   10.1016/J.YJMCC.2007.07.045.
770 Hashimoto K. 2021. Repurposing of CNS drugs to treat COVID-19 infection: targeting the
771   sigma-1 receptor. *European Archives of Psychiatry and Clinical Neuroscience* 271:249–
772   258. DOI: 10.1007/s00406-020-01231-x.
773 Hayashi T. 2015. Sigma-1 receptor: The novel intracellular target of neuropsychotherapeutic
774   drugs. *Journal of Pharmacological Sciences* 127:2–5. DOI: 10.1016/j.jphs.2014.07.001.
775 Hayashi T, Rizzuto R, Hajnoczky G, Su TP. 2009. MAM: more than just a housekeeper. *Trends*
776   *in Cell Biology* 19:81–88. DOI: 10.1016/j.tcb.2008.12.002.
777 Hayashi T, Su TP. 2003a. σ-1 receptors (σ1 binding sites) form raft-like microdomains and target
778   lipid droplets on the endoplasmic reticulum: Roles in endoplasmic reticulum lipid
779   compartmentalization and export. *Journal of Pharmacology and Experimental Therapeutics*
780   306:718–725. DOI: 10.1124/jpet.103.051284.
781 Hayashi T, Su TP. 2003b. σ-1 receptors (σ1 binding sites) form raft-like microdomains and
782   target lipid droplets on the endoplasmic reticulum: Roles in endoplasmic reticulum lipid

783   compartmentalization and export. *Journal of Pharmacology and Experimental Therapeutics*
784   306:718–725. DOI: 10.1124/jpet.103.051284.
785 Hayashi T, Su TP. 2007. Sigma-1 Receptor Chaperones at the ER- Mitochondrion Interface
786   Regulate Ca2+ Signaling and Cell Survival. *Cell* 131:596–610. DOI:
787   10.1016/J.CELL.2007.08.036.
788 Hirano K, Tagashira H, Fukunaga K. 2014. Cardioprotective Effect of the Selective Sigma-1
789   Receptor Agonist, SA4503. *YAKUGAKU ZASSHI* 134:707–713. DOI: 10.1248/yakushi.13-
790   00255-3.
791 Hoertel N, Sánchez-Rico M, Vernet R, Jannot A-S, Neuraz A, Blanco C, Lemogne C, Airagnes
792   G, Paris N, Daniel C, Gramfort A, Lemaitre G, Bernaux M, Bellamine A, Beeker N,
793   Limosin F. 2021. Observational study of haloperidol in hospitalized patients with COVID-
794   19. *PLOS ONE* 16:e0247122. DOI: 10.1371/journal.pone.0247122.
795 Huang C, Wang Y, Li X, Ren L, Zhao J, Hu Y, Zhang L, Fan G, Xu J, Gu X, Cheng Z, Yu T,
796   Xia J, Wei Y, Wu W, Xie X, Yin W, Li H, Liu M, Xiao Y, Gao H, Guo L, Xie J, Wang G,
797   Jiang R, Gao Z, Jin Q, Wang J, Cao B. 2020. Clinical features of patients infected with
798   2019 novel coronavirus in Wuhan, China. *The Lancet* 395:497–506. DOI: 10.1016/S0140-
799   6736(20)30183-5.
800 Janssen SPM, Gayan-Ramirez G, Van Den Bergh A, Herijgers P, Maes K, Verbeken E,
801   Decramer M. 2005. Interleukin-6 causes myocardial failure and skeletal muscle atrophy in
802   rats. *Circulation* 111:996–1005. DOI: 10.1161/01.CIR.0000156469.96135.0D.
803 Karakikes I, Ameen M, Termglinchan V, Wu JC. 2015. Human Induced Pluripotent Stem Cell-
804   Derived Cardiomyocytes: Insights into Molecular, Cellular, and Functional Phenotypes.
805   *Circulation Research* 117:80–88. DOI: 10.1161/CIRCRESAHA.117.305365.
806 Krenz M, Robbins J. 2004. Impact of beta-myosin heavy chain expression on cardiac function
807   during stress. *Journal of the American College of Cardiology* 44:2390–2397. DOI:
808   10.1016/J.JACC.2004.09.044.
809 Lenze EJ, Mattar C, Zorumski CF, Stevens A, Schweiger J, Nicol GE, Miller JP, Yang L,
810   Yingling M, Avidan MS, Reiersen AM. 2020. Fluvoxamine vs Placebo and Clinical
811   Deterioration in Outpatients With Symptomatic COVID-19. *JAMA* 324:2292. DOI:
812   10.1001/jama.2020.22760.
813 Lewis R, Li J, McCormick PJ, Huang CL-H, Jeevaratnam K. 2020. Is the sigma-1 receptor a
814   potential pharmacological target for cardiac pathologies? A systematic review. *International
815   Journal of Cardiology. Heart & Vasculature* 26. DOI: 10.1016/J.IJCHA.2019.100449.
816 Lindner D, Fitzek A, Bräuninger H, Aleshcheva G, Edler C, Meissner K, Scherschel K, Kirchhof
817   P, Escher F, Schultheiss HP, Blankenberg S, Püschel K, Westermann D. 2020. Association
818   of Cardiac Infection with SARS-CoV-2 in Confirmed COVID-19 Autopsy Cases. *JAMA
819   Cardiology*. DOI: 10.1001/jamacardio.2020.3551.
820 Lovato ECW, Barboza LN, Wietzikoski S, de Souza ANV, Auth PA, Junior AG, Dos Reis
821   Lívero FA. 2020. Repurposing Drugs for the Management of Patients with Confirmed
822   Coronavirus Disease 2019 (COVID-19). *Current pharmaceutical design*. DOI:
823   10.2174/1381612826666200707121636.
824 Magadum A, Kishore R. 2020. Cardiovascular Manifestations of COVID-19 Infection. *Cells*
825   9:2508. DOI: 10.3390/cells9112508.
826 Marchiano S, Hsiang T-Y, Khanna A, Higashi T, Whitmore LS, Bargehr J, Davaapil H, Chang J,
827   Smith E, Ong LP, Colzani M, Reinecke H, Yang X, Pabon L, Sinha S, Najafian B,
828   Sniadecki NJ, Bertero A, Gale M, Murry CE. 2021. SARS-CoV-2 infects human pluripotent

829   stem cell-derived cardiomyocytes, impairing electrical and mechanical function. *Stem Cell*
830   *Reports*:2020.08.30.274464. DOI: 10.1016/j.stemcr.2021.02.008.
831   Morales-Lázaro SL, González-Ramírez R, Rosenbaum T. 2019. Molecular interplay between the
832   sigma-1 receptor, steroids, and ion channels. *Frontiers in Pharmacology* 10. DOI:
833   10.3389/fphar.2019.00419.
834   Nguyen E, McCracken K, Liu Y, Pouw B, Matsumoto R. 2005. Involvement of sigma (sigma)
835   receptors in the acute actions of methamphetamine: receptor binding and behavioral studies.
836   *Neuropharmacology* 49:638–645. DOI: 10.1016/J.NEUROPHARM.2005.04.016.
837   Niehoff J, Matzkies M, Nguemo F, Hescheler J, Reppel M. 2019. The Effect of Antiarrhythmic
838   Drugs on the Beat Rate Variability of Human Embryonic and Human Induced Pluripotent
839   Stem Cell Derived Cardiomyocytes. *Scientific Reports* 9:1–10. DOI: 10.1038/s41598-019-
840   50557-7.
841   Novakova M, Ela C, Barg J, Vogel Z, Hasin Y, Eilam Y. 1995. Inotropic action of σ receptor
842   ligands in isolated cardiac myocytes from adult rats. *European Journal of Pharmacology*
843   286:19–30. DOI: 10.1016/0014-2999(95)00424-J.
844   Novakova M, Sedlakova B, Sirova M, Fialova K, Krizanova O. 2010. Haloperidol increases
845   expression of the inositol 1,4,5-trisphosphate receptors in rat cardiac atria, but not in
846   ventricles. *General Physiology and Biophysics* 29:381–389. DOI:
847   10.4149/gpb_2010_04_381.
848   Okuyama S, Imagawa Y, Ogawa S ichi, Araki H, Ajima A, Tanaka M, Muramatsu M, Nakazato
849   A, Yamaguchi K, Yoshida M, Otomo S. 1993. NE-100, a novel sigma receptor ligand: In
850   vivo tests. *Life Sciences* 53. DOI: 10.1016/0024-3205(93)90588-T.
851   Oslowski CM, Urano F. 2011. Measuring ER stress and the unfolded protein response using
852   mammalian tissue culture system. *Methods in enzymology* 490:71. DOI: 10.1016/B978-0-
853   12-385114-7.00004-0.
854   Page RL, O'bryant CL, Cheng D, Dow TJ, Ky B, Stein CM, Spencer AP, Trupp RJ, Lindenfeld
855   JA. 2016. Drugs that may cause or exacerbate heart failure. *Circulation* 134:e32–e69. DOI:
856   10.1161/CIR.0000000000000426.
857   Pellicori P, Doolub G, Wong CM, Lee KS, Mangion K, Ahmad M, Berry C, Squire I, Lambiase
858   PD, Lyon A, McConnachie A, Taylor RS, Cleland JGF. 2021. COVID-19 and its
859   cardiovascular effects: a systematic review of prevalence studies. *Cochrane Database of
860   Systematic Reviews* 2021. DOI: 10.1002/14651858.CD013879.
861   Perez-Bermejo JA, Kang S, Rockwood SJ, Simoneau CR, Joy DA, Silva AC, Ramadoss GN,
862   Flanigan WR, Fozouni P, Li H, Chen P-Y, Nakamura K, Whitman JD, Hanson PJ,
863   McManus BM, Ott M, Conklin BR, McDevitt TC. 2021. SARS-CoV-2 infection of human
864   iPSC-derived cardiac cells reflects cytopathic features in hearts of patients with COVID-19.
865   *Science Translational Medicine*:eabf7872. DOI: 10.1126/scitranslmed.abf7872.
866   Pointon A, Harmer AR, Dale IL, Abi-Gerges N, Bowes J, Pollard C, Garside H. 2015.
867   Assessment of cardiomyocyte contraction in human-induced pluripotent stem cell-derived
868   cardiomyocytes. *Toxicological Sciences* 144:227–237. DOI: 10.1093/toxsci/kfu312.
869   Qin J, Wang P, Li Y, Yao L, Liu Y, Yu T, Lin J, Fang X, Huang Z. 2019. Activation of Sigma-1
870   Receptor by Cutamesine Attenuates Neuronal Apoptosis by Inhibiting Endoplasmic
871   Reticulum Stress and Mitochondrial Dysfunction in a Rat Model of Asphyxia Cardiac
872   Arrest. *Shock (Augusta, Ga.)* 51:105–113. DOI: 10.1097/SHK.0000000000001119.
873   Ramakers C, Ruijter JM, Lekanne Deprez RH, Moorman AFM. 2003. Assumption-free analysis
874   of quantitative real-time polymerase chain reaction (PCR) data. *Neuroscience Letters*

875   339:62–66. DOI: 10.1016/S0304-3940(02)01423-4.
876 Reznikov LR, Norris MH, Vashisht R, Bluhm AP, Li D, Liao YSJ, Brown A, Butte AJ, Ostrov
877   DA. 2020. Identification of antiviral antihistamines for COVID-19 repurposing.
878   *Biochemical and Biophysical Research Communications*. DOI: 10.1016/j.bbrc.2020.11.095.
879 Ritzenthaler C, Elamawi R. 2006. The ER in replication of positive-strand RNA viruses. *Plant*
880   *Cell Monographs* 4:309–330. DOI: 10.1007/7089_061.
881 Rosen DA, Seki SM, Fernández-Castañeda A, Beiter RM, Eccles JD, Woodfolk JA, Gaultier A.
882   2019. Modulation of the sigma-1 receptor-IRE1 pathway is beneficial in preclinical models
883   of inflammation and sepsis. *Science Translational Medicine* 11. DOI:
884   10.1126/scitranslmed.aau5266.
885 Rothenbacher D, Müller-Scholze S, Herder C, Koenig W, Kolb H. 2006. Differential expression
886   of chemokines, risk of stable coronary heart disease, and correlation with established
887   cardiovascular risk markers. *Arteriosclerosis, Thrombosis, and Vascular Biology* 26:194–
888   199. DOI: 10.1161/01.ATV.0000191633.52585.14.
889 Rousseaux CG, Greene SF. 2016. Sigma receptors [σ Rs]: Biology in normal and diseased
890   states. *Journal of Receptors and Signal Transduction* 36:327–388. DOI:
891   10.3109/10799893.2015.1015737.
892 Ruijter JM, Ramakers C, Hoogaars WMH, Karlen Y, Bakker O, van den hoff MJB, Moorman
893   AFM. 2009. Amplification efficiency: Linking baseline and bias in the analysis of
894   quantitative PCR data. *Nucleic Acids Research* 37. DOI: 10.1093/nar/gkp045.
895 Seftel D, Boulware DR. 2021. Prospective Cohort of Fluvoxamine for Early Treatment of
896   Coronavirus Disease 19. *Open Forum Infectious Diseases* 8. DOI: 10.1093/ofid/ofab050.
897 Sequeira V, Nijenkamp LLAM, Regan JA, Van Der Velden J. 2014. The physiological role of
898   cardiac cytoskeleton and its alterations in heart failure. *Biochimica et Biophysica Acta -*
899   *Biomembranes* 1838:700–722. DOI: 10.1016/j.bbamem.2013.07.011.
900 Sharma A, Garcia G, Wang Y, Plummer JT, Morizono K, Arumugaswami V, Svendsen CN.
901   2020. Human iPSC-Derived Cardiomyocytes Are Susceptible to SARS-CoV-2 Infection.
902   *Cell Reports Medicine* 1:100052. DOI: 10.1016/j.xcrm.2020.100052.
903 Sharma A, McKeithan WL, Serrano R, Kitani T, Burridge PW, Álamo JC del, Mercola M, Wu
904   JC. 2018. Use of human induced pluripotent stem cell–derived cardiomyocytes to assess
905   drug cardiotoxicity. *Nature Protocols 2018 13:12* 13:3018–3041. DOI: 10.1038/s41596-
906   018-0076-8.
907 Shi S, Qin M, Shen B, Cai Y, Liu T, Yang F, Gong W, Liu X, Liang J, Zhao Q, Huang H, Yang
908   B, Huang C. 2020. Association of Cardiac Injury with Mortality in Hospitalized Patients
909   with COVID-19 in Wuhan, China. *JAMA Cardiology* 5. DOI:
910   10.1001/jamacardio.2020.0950.
911 Shinoda Y, Tagashira H, Bhuiyan MS, Hasegawa H, Kanai H, Fukunaga K. 2016a. Haloperidol
912   aggravates transverse aortic constriction-induced heart failure via mitochondrial
913   dysfunction. *Journal of Pharmacological Sciences* 131:172–183. DOI:
914   10.1016/j.jphs.2016.05.012.
915 Shinoda Y, Tagashira H, Bhuiyan MS, Hasegawa H, Kanai H, Zhang C, Han F, Fukunaga K.
916   2016b. Corticosteroids mediate heart failure-induced depression through reduced σ1-
917   receptor expression. *PLoS ONE* 11. DOI: 10.1371/journal.pone.0163992.
918 Stracina T, Novakova M. 2018. Cardiac sigma receptors - An update. *Physiological Research*
919   67:S561–S576. DOI: 10.33549/physiolres.934052.
920 Stringer C, Wang T, Michaelos M, Pachitariu M. 2021. Cellpose: a generalist algorithm for

921   cellular segmentation. *Nature Methods* 18:100–106. DOI: 10.1038/s41592-020-01018-x.

922   Su TP, Hayashi T, Maurice T, Buch S, Ruoho AE. 2010. The sigma-1 receptor chaperone as an

923   inter-organelle signaling modulator. *Trends in Pharmacological Sciences* 31:557–566. DOI:

924   10.1016/j.tips.2010.08.007.

925   Szabo A, Kovacs A, Frecska E, Rajnavolgyi E. 2014. Psychedelic N,N-dimethyltryptamine and

926   5-methoxy-N,N-dimethyltryptamine modulate innate and adaptive inflammatory responses

927   through the sigma-1 receptor of human monocyte-derived dendritic cells. *PloS one*

928   9:e106533. DOI: 10.1371/journal.pone.0106533.

929   Tagashira H, Bhuiyan MS, Shioda N, Fukunaga K. 2014. Fluvoxamine rescues mitochondrial

930   Ca2 + transport and ATP production through σ1-receptor in hypertrophic cardiomyocytes.

931   *Life Sciences* 95:89–100. DOI: 10.1016/j.lfs.2013.12.019.

932   Tagashira H, Fukunaga K. 2012. Cardioprotective Effect of Fluvoxamine, Sigma-1 Receptor

933   High Affinity Agonist. *YAKUGAKU ZASSHI* 132:167–172. DOI: 10.1248/yakushi.132.167.

934   Tagashira H, Zhang C, Lu YM, Hasegawa H, Kanai H, Han F, Fukunaga K. 2013. Stimulation of

935   σ1-receptor restores abnormal mitochondrial Ca2 + mobilization and ATP production

936   following cardiac hypertrophy. *Biochimica et Biophysica Acta - General Subjects*

937   1830:3082–3094. DOI: 10.1016/j.bbagen.2012.12.029.

938   Tarabová B, Nováková M, Lacinová L. 2009. Haloperidol moderately inhibits cardiovascular L-

939   type calcium current. *General Physiology and Biophysics* 28:249–259. DOI:

940   10.4149/gpb_2009_03_249.

941   Towbin H, Gordon J, Staehelin T. 1989. Immunoblotting in the Clinical Laboratory. *Journal of*

942   *Clinical Chemistry and Laboratory Medicine* 27:495–502. DOI:

943   10.1515/cclm.1989.27.8.495.

944   Tummino TA, Rezelj V V., Fischer B, Fischer A, O'Meara MJ, Monel B, Vallet T, White KM,

945   Zhang Z, Alon A, Schadt H, O'Donnell HR, Lyu J, Rosales R, McGovern BL,

946   Rathnasinghe R, Jangra S, Schotsaert M, Galarneau J-R, Krogan NJ, Urban L, Shokat KM,

947   Kruse AC, García-Sastre A, Schwartz O, Moretti F, Vignuzzi M, Pognan F, Shoichet BK.

948   2021. Drug-induced phospholipidosis confounds drug repurposing for SARS-CoV-2.

949   *Science* 373:541–547. DOI: 10.1126/SCIENCE.ABI4708.

950   Vela JM. 2020. Repurposing Sigma-1 Receptor Ligands for COVID-19 Therapy? *Frontiers in*

951   *Pharmacology* 11:1716. DOI: 10.3389/fphar.2020.582310.

952   Wang S, Binder P, Fang Q, Wang Z, Xiao W, Liu W, Wang X. 2018. Endoplasmic reticulum

953   stress in the heart: insights into mechanisms and drug targets. *British Journal of*

954   *Pharmacology* 175:1293. DOI: 10.1111/BPH.13888.

955   Watkins SJ, Borthwick GM, Oakenfull R, Robson A, Arthur HM. 2012. Angiotensin II-induced

956   cardiomyocyte hypertrophy in vitro is TAK1-dependent and Smad2/3-independent.

957   *Hypertension Research* 35:393–398. DOI: 10.1038/hr.2011.196.

958   Witchel HJ. 2011. Drug-induced hERG Block and Long QT Syndrome. *Cardiovascular*

959   *Therapeutics* 29:251–259. DOI: 10.1111/j.1755-5922.2010.00154.x.

960   Wong CK, Luk HKH, Lai WH, Lau YM, Zhang RR, Wong ACP, Lo GCS, Chan KH, Hung IFN,

961   Tse HF, Woo PCY, Lau SKP, Siu CW. 2020. Human-induced pluripotent stem cell-derived

962   cardiomyocytes platform to study SARS-CoV-2 related myocardial injury. *Circulation*

963   *Journal* 84:2027–2031. DOI: 10.1253/circj.CJ-20-0881.

964   Wu L, O'Kane AM, Peng H, Bi Y, Motriuk-Smith D, Ren J. 2020. SARS-CoV-2 and

965   cardiovascular complications: From molecular mechanisms to pharmaceutical management.

966   *Biochemical Pharmacology* 178. DOI: 10.1016/j.bcp.2020.114114.

967   Yang J, Zheng Y, Gou X, Pu K, Chen Z, Guo Q, Ji R, Wang H, Wang Y, Zhou Y. 2020.
968   Prevalence of comorbidities and its effects in coronavirus disease 2019 patients: A
969   systematic review and meta-analysis. *International Journal of Infectious Diseases* 94:91–
970   95. DOI: 10.1016/j.ijid.2020.03.017.
971   Yao XH, Li TY, He ZC, Ping YF, Liu HW, Yu SC, Mou HM, Wang LH, Zhang HR, Fu WJ,
972   Luo T, Liu F, Chen C, Xiao HL, Guo HT, Lin S, Xiang DF, Shi Y, Li QR, Huang X, Cui Y,
973   Li XZ, Tang W, Pan PF, Huang XQ, Ding YQ, Bian XW. 2020. [A pathological report of
974   three COVID-19 cases by minimally invasive autopsies]. *Zhonghua bing li xue za zhi =*
975   *Chinese journal of pathology* 49:E009. DOI: 10.3760/cma.j.cn112151-20200312-00193.
976   Youker K, Smith CW, Anderson DC, Miller D, Michael LH, Rossen RD, Entman ML. 1992.
977   Neutrophil adherence to isolated adult cardiac myocytes: Induction by cardiac lymph
978   collected during ischemia and reperfusion. *Journal of Clinical Investigation* 89:602–609.
979   DOI: 10.1172/JCI115626.
980   Zhou R, Chen SH, Li G, Chen HL, Liu YX, Wu HM, Wang Y, Feng J, Hong JS. 2019. Ultralow
981   doses of dextromethorphan protect mice from endotoxin-induced sepsis-like hepatotoxicity.
982   *Chemico-Biological Interactions* 303:50–56. DOI: 10.1016/j.cbi.2019.02.025.
983

Figure 1

Human induced pluripotent stem cell-derived cardiomyocytes (hiPSC-CMs) express 850
the Sigma-1 receptor (S1R).

(A) End point PCR analysis of S1R on mRNA isolated from three hiPSC-CMs replicate samples
from three independent batches of differentiation (N=3). GAPDH was used as housekeeping
control of mRNA samples. Uncropped agarose gel is appended in Supplemental Figure S5
with appropriate controls. (B) Representative western blot of S1R expression in protein
extracts of control hiPSC-CMs. Actin was used as a loading control. The detection of the
protein was performed in samples from 3 different batches with similar results (N=3). Full-
length gels of the representative blots shown here are presented in Supplemental Figure S5.
(C) Representative image of staining performed in fixed cardiomyocytes from 3 different
batches shows S1R presence and similar distribution in hiPSC-CMs (N=3). S1R (green);
phalloidin (red) and nuclei (blue); scale bar = 50 μm. (D) Immunofluorescence shows
mitochondrial marker VDAC1/Porin (red) and S1R (green) in hiPSC-CMs. Representative
image of 3 independent experiments (N=3). Nuclei were stained with DAPI (blue); scale bar =
50 μm. (E) Immunofluorescence shows ER chaperone lectin Calnexin (CNX) (red) and S1R
(green) in hiPSC-CMs. Representative image of 3 independent experiments (N=3). Nuclei
were stained with DAPI (blue); scale bar = 50 μm. Zoom-in highlights the cells indicated by
the arrowheads (D and E).
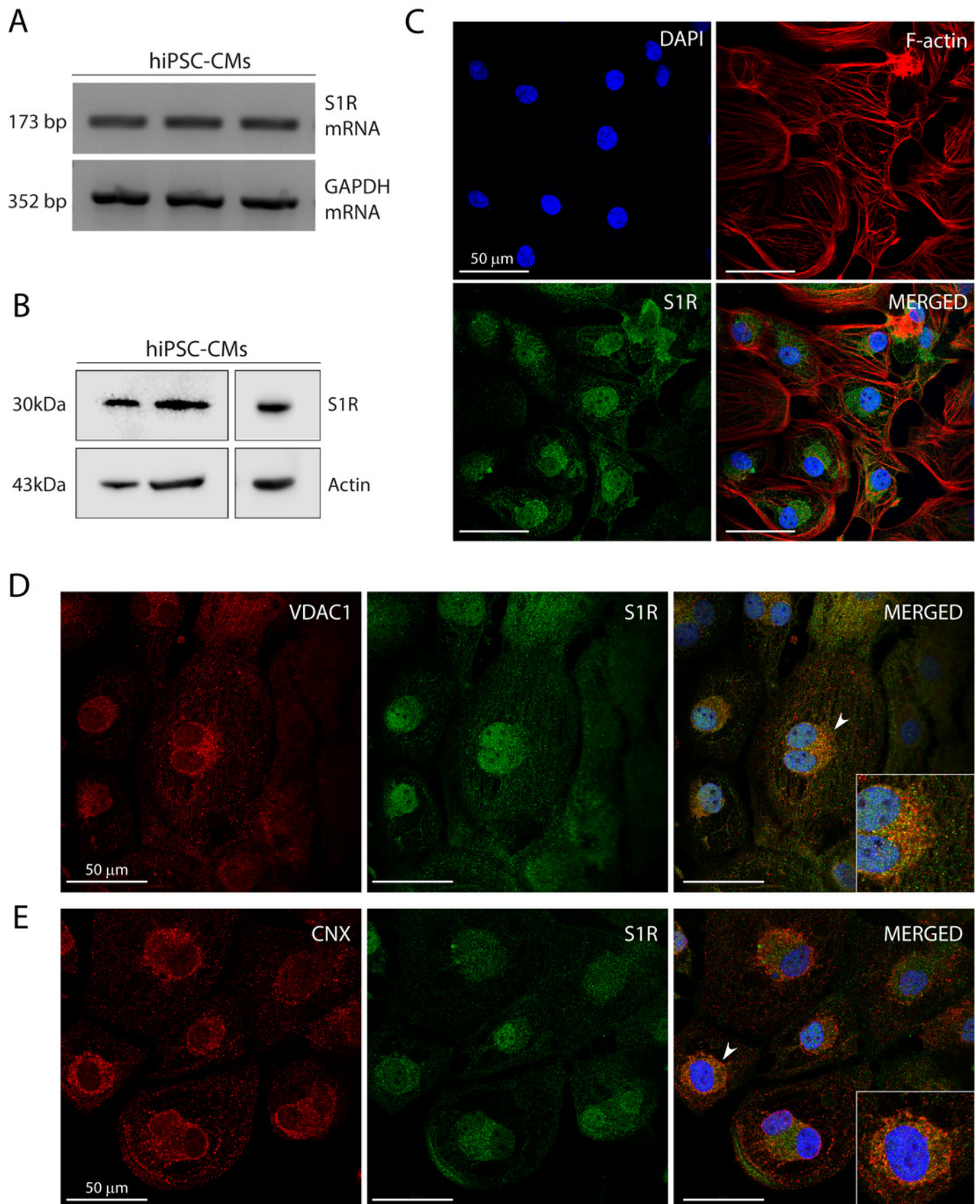
Figure 2

S1R inhibition reduces SARS-CoV-2 infection, replication, and cytotoxicity in hiPSC-CMs

(A) hiPSC-CMs were pre-treated for 24 h with 1 µM NE-100 and infected with SARS-CoV-2 at multiplicity of infection (MOI) of 0.1. Cells were evaluated at 48 hours post-infection (h.p.i). Representative immunostaining images show infected hiPSC-CMs positively stained for convalescent serum (CS) in red and no signal detection in mock conditions (N=3); scale bar = 100 µm. (B) The percentage of infected hiPSC-CMs was assessed by quantification of CS positive cells in SARS-CoV-2-infected and mock-infected conditions exposed or not to S1R high-affinity antagonist NE-100 (N=3). (C) Plaque forming units assay for the supernatants of the SARS-CoV-2 infected hiPSC-CMs (N=4). (D) Cell death was measured in the supernatant by LDH activity at 24, 48 (N=3) and 72 h.p.i (N=2). Data are represented as the mean ± S.E.M, analyzed by Nested t-test (p=0.0003) (B), unpaired two-tailed Welch's t-test (p=0.0336) (C) and ordinary one-way ANOVA followed by Holm-Sidak's post-hoc (24h p=0.0089; 48h p<0.0001 and p=0.0001) (D). Data points represent independent experiments.*p<0.05, **p<0.01, ***p<0.001, **** p < 0.0001.
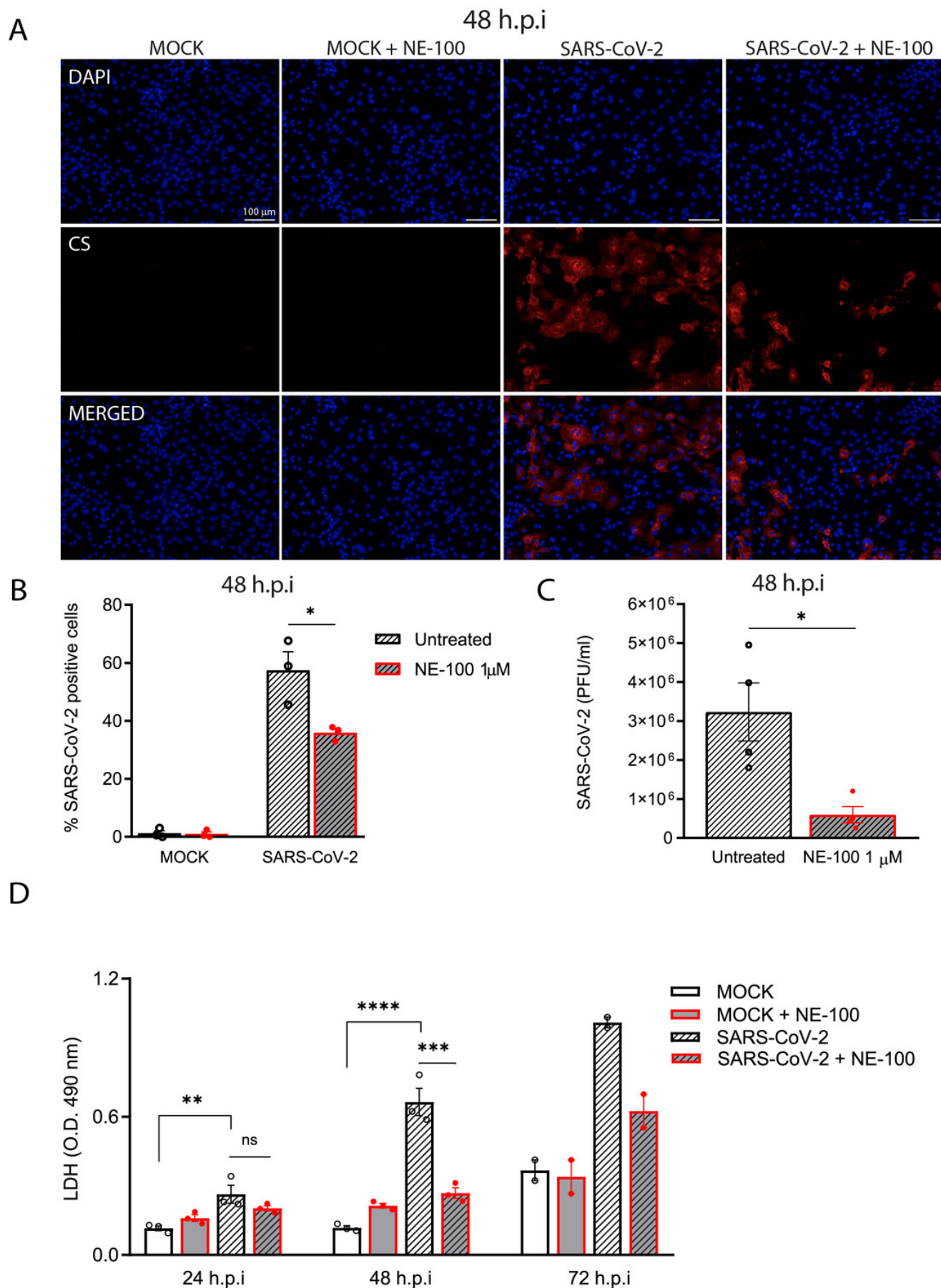
Figure 3

NE-100 decreases cytokine release that follows SARS-CoV-2 infection in hiPSC-CMs

(A and B) hiPSC- hiPSC-CMs were pre-treated or not with NE-100 1 µM and infected with SARS-CoV-2. Supernatants were analyzed by ELISA for IL-6, IL-8 and TNF-α at 24 h.p.i (IL-6 p=0.0006 and p=0.0395; IL-8 p=0.0661 and p=0.1426; TNF-α p=0.0033 and p=0.0077) (A) and 48 h.p.i (IL-6 p<0.0001 and p=0.0009; IL-8 p=0.0001 and p=0.0017; TNF-α p=0.1663 and p=0.5359) (B) (N=3). Data were normalized to the mean control value of each experiment and represents the mean ± SEM of fold increase, analyzed by ordinary one-way ANOVA with Holm-Sidak's post-hoc. Data points represent independent experiments. *p<0.05, **p<0.01, ***p<0.001, **** p < 0.0001.

A

B
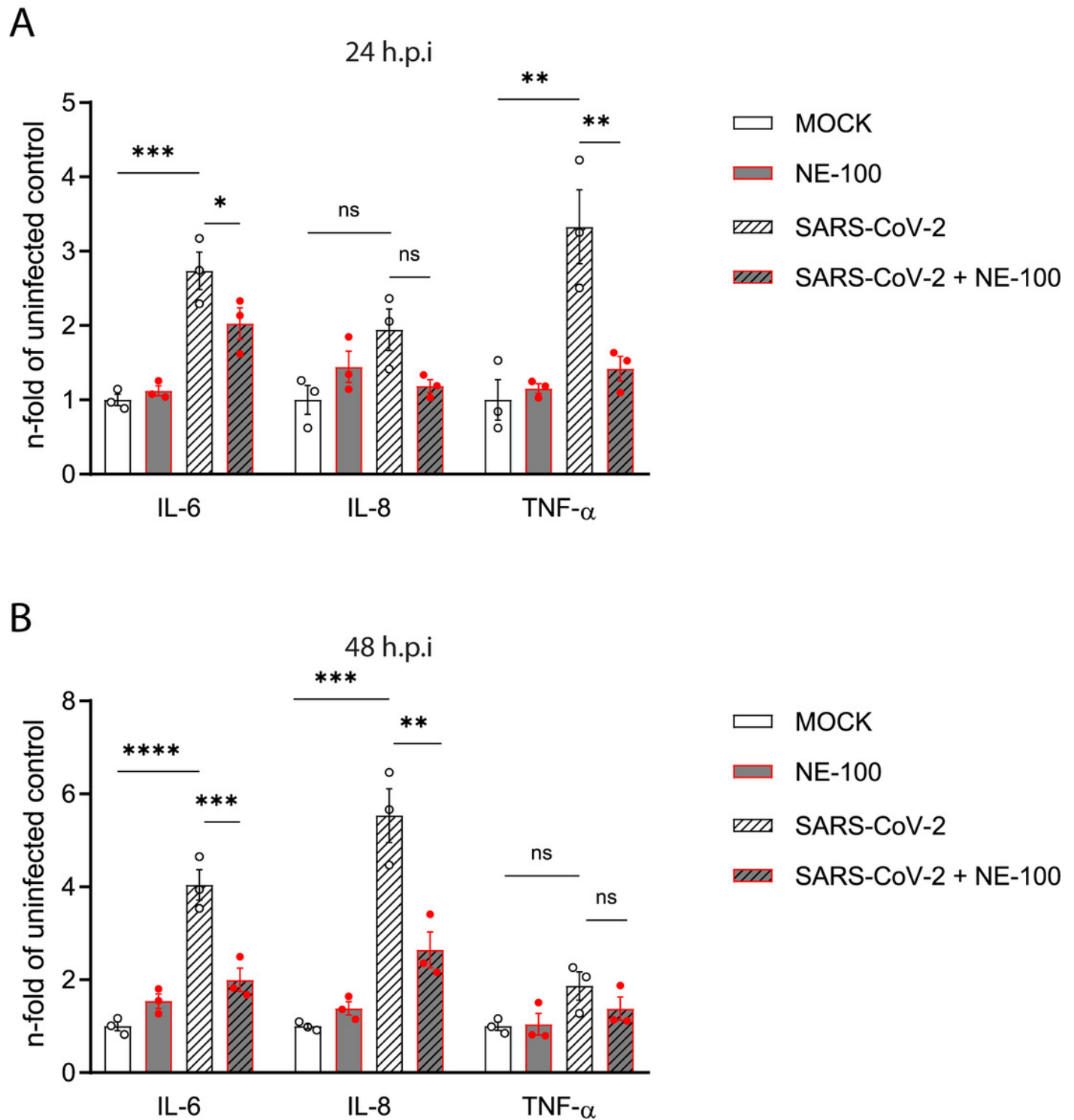
Figure 4

NE-100 does not induce death and ER stress but decreases beating frequency in hiPSC-CMs

(A) Neutral red cell viability assay for escalating NE-100 concentrations shows non-significant changes after 72 hours post-treatment. Data are represented as the baseline-corrected mean ± S.E.M relative to the vehicle condition analyzed by one-way ANOVA (N=3). (B) Nuclear size analysis by DAPI staining shows the percentage of pyknotic nuclei after 48 h (N=3); Dots represent the percentage of each well evaluated in three independent experiments analyzed by unpaired Welch's t test; non-significant (p=0.1738). (C) Normalized mRNA expression of spliced and unspliced XBP1 transcripts in samples from different batches exposed to NE-100 1 μM in four independent experiments (N=4). Data are expressed relative to total XBP1 normalized expression ± S.E.M and were analyzed by multiple t-tests (Holm-Sidak method) (spliced/total p= 0.7338 and unspliced/total p= 0.6943). (D) CHOP mRNA in samples from different batches exposed to NE-100 1 μM in three independent experiments (N=3). Values are expressed as fold-change relative to the untreated condition ± S.E.M and were analyzed by unpaired Welch's t test; non-significant (p=0.5512). (E) Average of beats per minute analyzed 24 and 48 h after exposure to NE-100 or vehicle (N=3). Data are presented as the average ± S.E.M, statistical differences were analyzed by multiple t-tests (Holm-Sidak method) (24h p=0.03663; 48h p=0.00349).
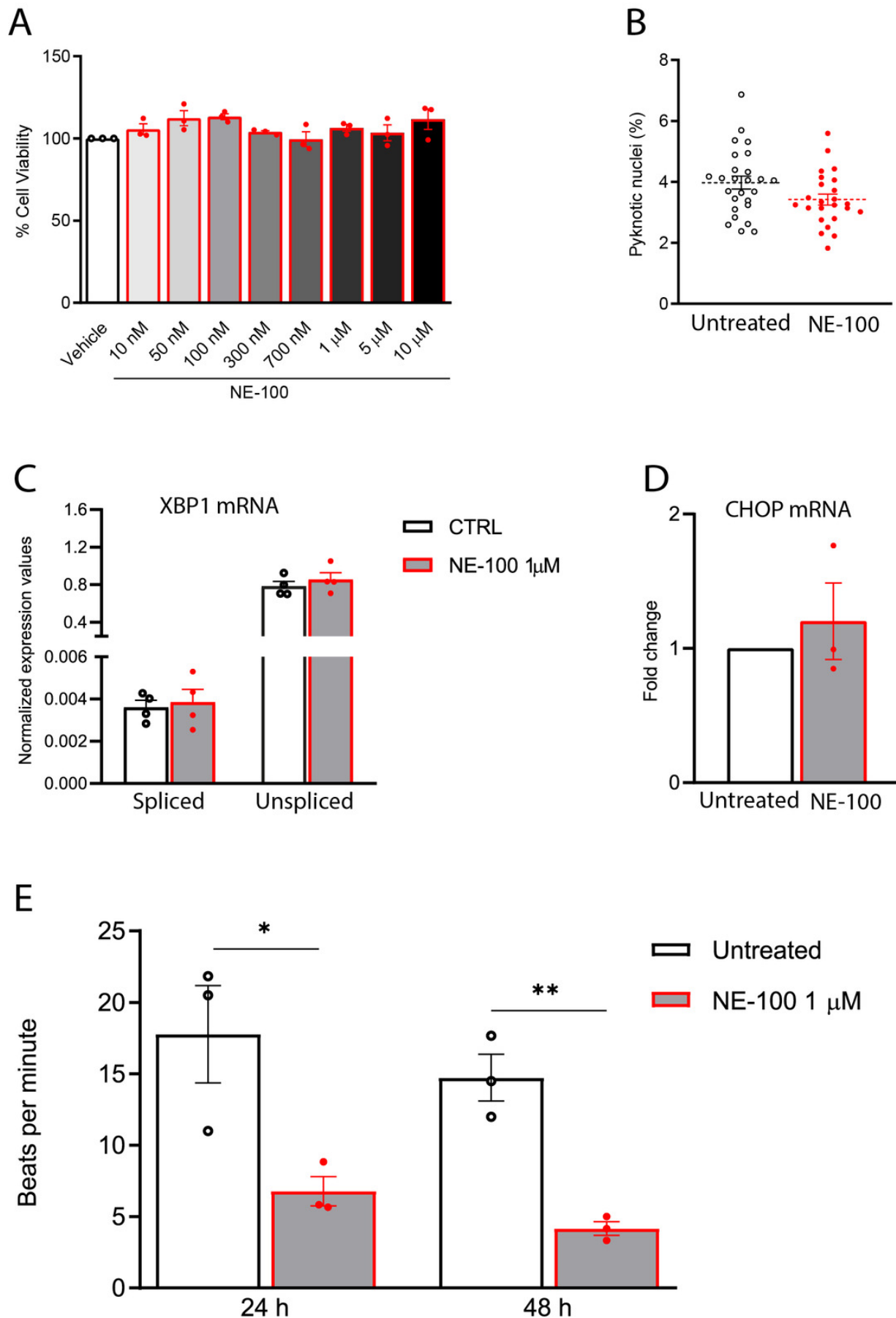
Figure 5

S1R inhibition downregulates the expression of structural-related genes and compromise cytoskeletal integrity

(A) Real-time qPCR shows decreased levels of transcript content for ANP after S1R inhibition (N=4). (B) Cell area was quantified by F-actin staining and shows a significant decrease in cell body sizes after exposure to NE-100 for 48 h. Data represents distribution of surface area measured from approximately 24000 cells in four independent experiments (N=4). (C) Changes in myofibril and cytoskeletal-related gene expression after 24h of NE-100 1 μM exposure from at least three replicates obtained from independent experiments (N=3 or N=4). (D and E) Quantification of cTnT immunoreactive area and intensity, normalized by the total number of cells per field; values are expressed relative to untreated controls (D) or arbitrary units, and data points represent mean cTnT intensity per well (E) (N=4). (F) Representative confocal images show in more detail the disruption of F-actin and cTnT organization, observed in at least four independent repeats (N=4). Scale bar = 50 μm. Data are presented as the average ± S.E.M, statistical differences were analyzed by unpaired Welch's t-test (p= 0.0081 and p=0.0262) (A and D), nested t-test (p=0.0108) (B), multiple t-tests (Holm-Sidak method) (*ACTN1* p= 0.8478, *ACTN2* p= 0.000004, *ACTA1* p<0.000001, *TNNI3* p=0.0011, *TNNT1* p=0.0001, *MYH6* p=0.0502, *MYH7* p=0.1582) (C), and Mann-Whitney test (p=0.0235) (E). Data points represent independent experiments unless otherwise stated. *p<0.05; **p<0.01; ***p<0.001; ****p<0.0001.